ACS Pharmacology & Translational Science

pubs.acs.org/ptsci Article

Structure and Dynamics of Adrenomedullin Receptors AM_1 and AM_2 Reveal Key Mechanisms in the Control of Receptor Phenotype by Receptor Activity-Modifying Proteins

Yi-Lynn Liang,[○] Matthew J. Belousoff,[○] Madeleine M. Fletcher,[○] Xin Zhang, Maryam Khoshouei, Giuseppe Deganutti, Cassandra Koole, Sebastian G. B. Furness, Laurence J. Miller, Debbie L. Hay, Arthur Christopoulos, Christopher A. Reynolds, Radostin Danev, Denise Wootten,* and Patrick M. Sexton*

Cite This: *ACS Pharmacol. Transl. Sci.* 2020, 3, 263−284 Read Online

ACCESS | Metrics & More | Article Recommendations | Supporting Information

ABSTRACT: Adrenomedullin (AM) and calcitonin gene-related peptide (CGRP) receptors are critically important for metabolism, vascular tone, and inflammatory response. AM receptors are also required for normal lymphatic and blood vascular development and angiogenesis. They play a pivotal role in embryo implantation and fertility and can provide protection against hypoxic and oxidative stress. CGRP and AM receptors are heterodimers of the calcitonin receptor-like receptor (CLR) and receptor activity-modifying protein 1 (RAMP1) (CGRPR), as well as RAMP2 or RAMP3 (AM_1R and AM_2R, respectively). However, the mechanistic basis for RAMP modulation of CLR phenotype is unclear. In this study, we report the cryo-EM structure of the AM_1R in complex with AM and Gs at a global resolution of 3.0 Å, and structures of the AM_2R in complex with either AM or intermedin/adrenomedullin 2 (AM2) and Gs at 2.4 and 2.3 Å, respectively. The structures reveal distinctions in the primary orientation of the extracellular domains (ECDs) relative to the receptor core and distinct positioning of extracellular loop 3 (ECL3) that are receptor-dependent. Analysis of dynamic data present in the cryo-EM micrographs revealed additional distinctions in the extent of mobility of the ECDs. Chimeric exchange of the linker region of the RAMPs connecting the TM helix and the ECD supports a role for this segment in controlling receptor phenotype. Moreover, a subset of the motions of the ECD appeared coordinated with motions of the G protein relative to the receptor core, suggesting that receptor ECD dynamics could influence G protein interactions. This work provides fundamental advances in our understanding of GPCR function and how this can be allosterically modulated by accessory proteins.

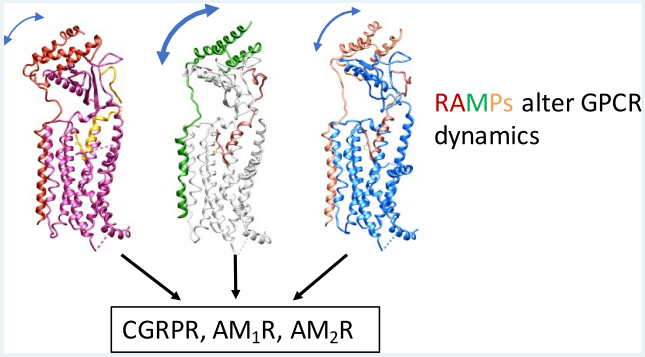

KEYWORDS: *cryo-electron microscopy, adrenomedullin, calcitonin gene-related peptide, G protein-coupled receptor, receptor activity-modifying protein, allosteric modulation, receptor structure−function*

G protein-coupled receptors (GPCRs) comprise the largest superfamily of cell surface receptors, and they are ubiquitously important for normal physiology, as well as key mediators of disease and disease resolution.[1,2] The complexity of GPCR function is further increased through interaction with accessory proteins that can modulate receptor phenotype. Prototypical of these accessory proteins is the receptor activity-modifying protein (RAMP) family of 3 single transmembrane spanning proteins, RAMP1−3, respectively.[3] There is increasing evidence that RAMPs can interact broadly with GPCRs,[3,4] but they are best studied for their interaction with the calcitonin (CT) family Class B GPCRs, the CT receptor (CTR), and CT receptor-like receptor (CLR), where they are responsible for formation of amylin receptors with CTR and the CT gene-related peptide (CGRP) and adrenomedullin (AM) receptors with CLR.[3,5] The CGRP receptor (CGRPR) is a heterodimer of CLR and RAMP1, while AM_1 and AM_2 receptors are heterodimers of CLR and RAMP2 or RAMP3, respectively.[3,5]

CGRP is a commonly expressed neuropeptide that performs a key role in sensory neurotransmission. It has wide-ranging physiological functions that include roles in metabolism, blood

Special Issue: Advances in GPCR Signal Transduction

Received: October 8, 2019
Published: March 20, 2020

https://dx.doi.org/10.1021/acsptsci.9b00080
ACS Pharmacol. Transl. Sci. 2020, 3, 263−284

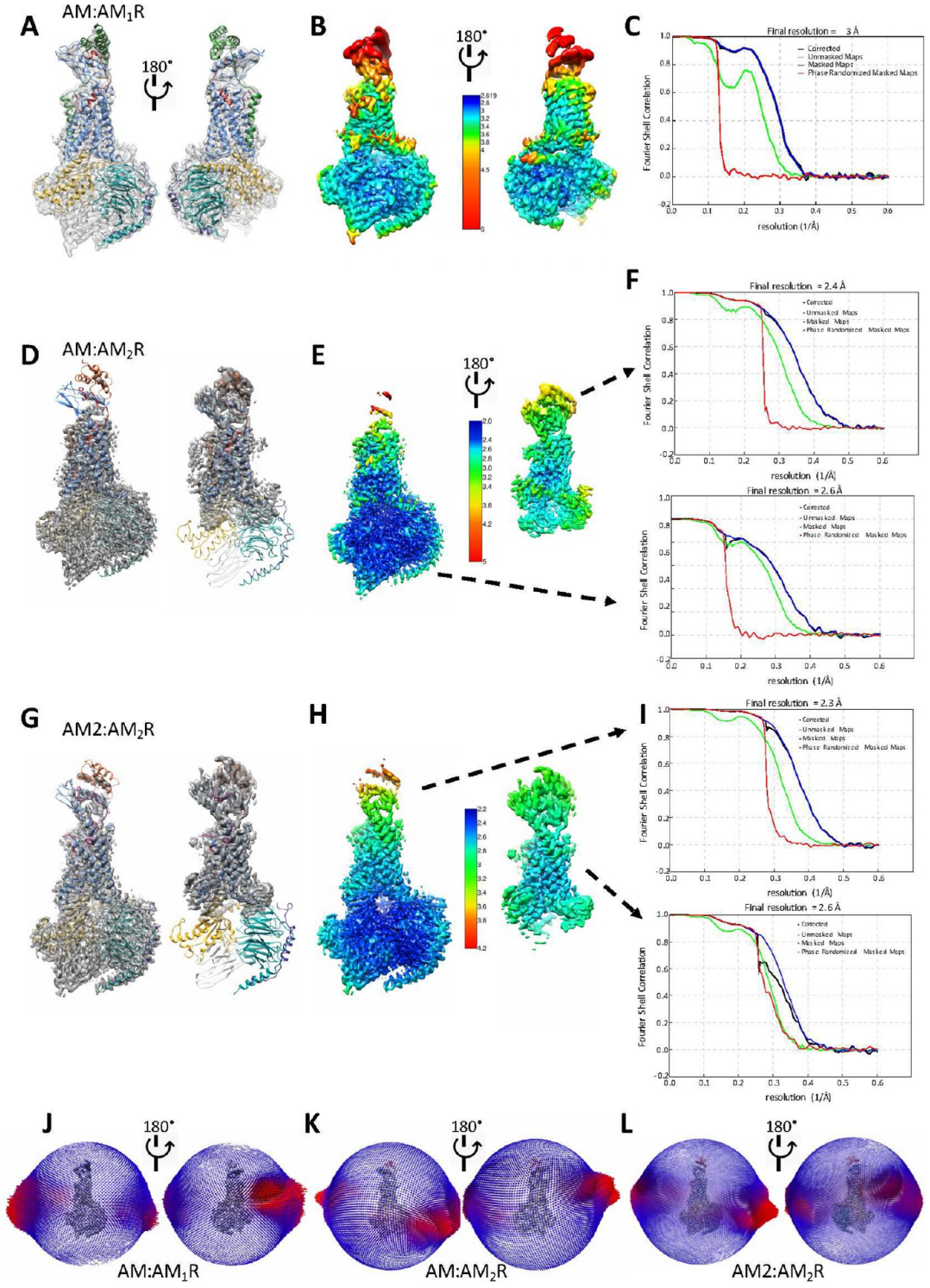

Figure 1. Refined EM maps of the AM receptor complexes. (A–C) AM:CLR:RAMP2:GsDN:Nb35 complex. (D–F) AM:CLR:-RAMP3:GsDN:Nb35 complex. (G–I) AM2:CLR:RAMP3:GsDN:Nb35 complex. (A, D, G) Full maps and receptor only maps (D, G) containing the backbone model of the complexes in ribbon format; CLR (blue), RAMP2 (green), RAMP3 (coral), AM (red), AM2 (dark pink), G protein α-subunit (gold), β-subunit (cyan), γ-subunit (dark purple), and Nb35 (white). (B, E, H) Local-resolution-filtered EM maps displaying local resolution (Å) colored from highest (dark blue) to lowest resolution (red). (C, F, I) Gold standard Fourier shell correlation (FSC) curves for the final maps and map validation from half maps, showing overall nominal resolutions of 3.0, 2.4, and 2.3 Å for the AM:AM$_1$R (C), AM:AM$_2$R (F), and AM2:AM$_2$R (I), respectively, and 2.6 Å for the receptor only maps (F, I). (J–L) 3D histogram representations of the Euler angle distribution of all the particles used in the reconstruction overlaid on the density map drawn on the same coordinate axis for complexes of the AM:AM$_1$R (J), AM:AM$_2$R (K), and AM2:AM$_2$R (L), respectively.

pressure regulation, inflammatory response, and auditory nerve development and function.[6−8] It is a potent vasodilator released during neurogenic inflammation. CGRP contributes to the pathology of migraine, with multiple antibody

https://dx.doi.org/10.1021/acsptsci.9b00080
ACS Pharmacol. Transl. Sci. 2020, 3, 263−284

therapeutics approved that either reduce levels of the peptide or inhibit its target receptor.[9] In contrast, CGRP is protective in experimental models of inflammatory bowel disease and hypertension, and it is a critical neuropeptide for development and modulation of auditory responses. Moreover, CGRP is reported to protect against HIV infection.[10,11]

AM, a potent vasodilator peptide hormone, is essential for normal physiology and development, with transgenic knockout of the peptide causing embryologic lethality.[12] It is required for normal lymphatic and blood vascular development and angiogenesis.[13] It plays a pivotal role in embryo implantation and fertility[14,15] and provides protection against hypoxic and oxidative stress.[16] Experimental manipulation of AM levels or AM receptor activity is indicative of protective roles in hypertension, myocardial infarction, and inflammatory disease, while AM peptides can also promote cancer growth and metastasis. A related peptide, intermedin/adrenomedullin 2 (AM2), also has a number of important regulatory functions and binds to the AM receptors.[5,17] Modulation of AM peptide signaling has significant therapeutic potential,[17−19] and an understanding of the structural basis for AM and AM2 binding to AM_1 and AM_2 receptors is required for rational exploitation of these targets.

We recently reported the structure of the CGRPR, and this revealed an unexpected interface for RAMP1 interaction with CLR and that the only direct interaction of RAMP1 with CGRP is limited to the peptide C-terminal residue,[20] first reported in isolated extracellular domains (ECDs) of CLR:RAMP1.[21] As such, the effect of RAMP1 on CLR pharmacology is predominantly allosteric. Mechanistic understanding of the allosteric control of CLR phenotype by different RAMPs requires structures of CLR with RAMP2 and RAMP3.

In this study, we report the cryo-EM structure of the AM_1R in complex with AM and Gs and structures of the AM_2R in complex with either AM or intermedin/adrenomedullin 2 (AM2) and Gs. The structures reveal distinctions in the primary orientation of the ECDs relative to the receptor core and distinctions in the position of extracellular loop 3 (ECL3) that are receptor-dependent. Analysis of dynamic data present in the micrographs revealed additional distinctions in the extent of mobility of the ECDs, and chimeric exchange of the linker region of the RAMPs connecting the transmembrane (TM) helix and the ECD supports a role for this segment in controlling receptor phenotype. Moreover, a subset of the motions of the ECD appeared coordinated with motions of the G protein relative to the receptor core, suggesting that receptor ECD dynamics could influence G protein interactions (and thus efficacy), which has been previously postulated but as-yet not demonstrated.[22,23]

RESULTS AND DISCUSSION

Structure Determination. The CLR expression construct previously used for determination of the CGRPR structure[20] was used to form complexes with RAMP2 (AM_1R) or RAMP3 (AM_2R). This construct had the native signal peptide substituted with that of hemagglutinin (HA) and affinity tags bracketed by 3C cleavage sites at the N- and C-terminus (FLAG and His, respectively). RAMP2 and RAMP3 were modified to include a HA signal sequence, followed by a FLAG epitope without a 3C cleavage site (Figure S1). These modifications did not alter receptor pharmacology (Figure S2A,B).

Active complexes of AM_1R or AM_2R with heterotrimeric Gs were formed following coexpression of CLR and RAMP2, or of CLR and RAMP3, with a stabilized form of Gαs, His-Gβ1, and Gγ2 in *Tni* insect cells.[20,24,25] Complex formation was initiated by addition of excess AM(13−52) (AM_1R and AM_2R) or AM2 (47 amino acid peptide) (AM_2R) and stabilized by removal of nucleotide with apyrase and addition of nanobody 35 (Nb35) that binds across the Gαs−Gβ1 interface.[26,27] The CLR affinity tags were cleaved with 3C enzyme, and the complex was solubilized in lauryl maltose neopentyl glycol (LMNG)/cholesteryl and then purified by nickel and anti-FLAG chromatography, followed by size-exclusion chromatography (SEC) to yield monodisperse peaks that contained each of the components of the complex with each of the peptide ligands (Figure S2C−H), with good 2D classes in negative stain transmission electron microscopy (TEM). Vitrified samples for each receptor complex were imaged by conventional cryo-TEM on a Titan Krios to yield consensus maps at gold standard FSC 0.143 of 3.0, 2.4, and 2.3 Å for the AM_AM_1R, AM_AM_2R, and AM2_AM_2R complexes, respectively (Figures 1A−I and S3A−C), despite varying levels of preferred orientation within the vitrified samples (Figure 1J−L). Focused refinement of the AM_2Rs using a mask around the receptor generated maps of 2.6 Å global resolution, with improved local resolution of the receptor ECD that allowed this domain to be directly modeled (Figures 1D−I and S3B,C).

High-resolution features were observed for each of the maps with local resolution ranging from 2.6 Å to >6 Å (AM_AM_1R), 2.0 Å to >4 Å (AM_AM_2R), and 2.2 Å to >4 Å (AM2_AM_2R) (Figures 1B,E,H and S4−S6), with highest resolution in the G protein, the G protein−CLR interface, and TM core for each of the receptors. Lower resolution was observed for the RAMP:CLR ECDs and associated peptide C-termini, with low resolution for the RAMP TM-ECD linker region and parts of ICL3 and ECL3 for each of the receptors (Figures S4−S6). No density was observed for most of the C-terminus of CLR, with limited density for C-terminal residues of the RAMPs (summarized in Figure S7). No clear density was observed for the N-terminal AM residue (S13) or for the N-terminal AM2 residues (T1-V8). The C-terminus of AM in the AM_1R ECD was poorly resolved. For this receptor, the backbone structure of the peptide in the ECD X-ray crystal structure (4RWF)[21] was used to assist in assigning the peptide density. In the case of the AM_2Rs, the maps from focused refinement allowed *ab initio* modeling of most of the ECD and peptide C-terminus. The C-terminal peptide backbones of AM and AM2 in the AM_2Rs were similar to those observed in related ECD X-ray crystal structures (4RWF[21] and 6D1U).[28] There was very limited density for the Gαs α-helical domain, and this was masked out in final refinements. Density for the C-terminal ends of Gβ1 and Gγ2 were variable across the receptors (Figures S4−S6). For the rest of the receptor and G protein the map density allowed robust assignment of side-chain rotamers using either the full map, or receptor focused maps (Figures S4−S6).

Global Structural Features of AM Receptors. While the ECDs of the complexes exhibited lower resolution in the consensus maps, the resolution did allow fitting of backbone models of the ECD of CLR and each of the RAMPs into the density to identify the primary metastable positions of these domains (Figure 2A,B). The AM and AM2 co-complexes of

https://dx.doi.org/10.1021/acsptsci.9b00080
ACS Pharmacol. Transl. Sci. 2020, 3, 263−284

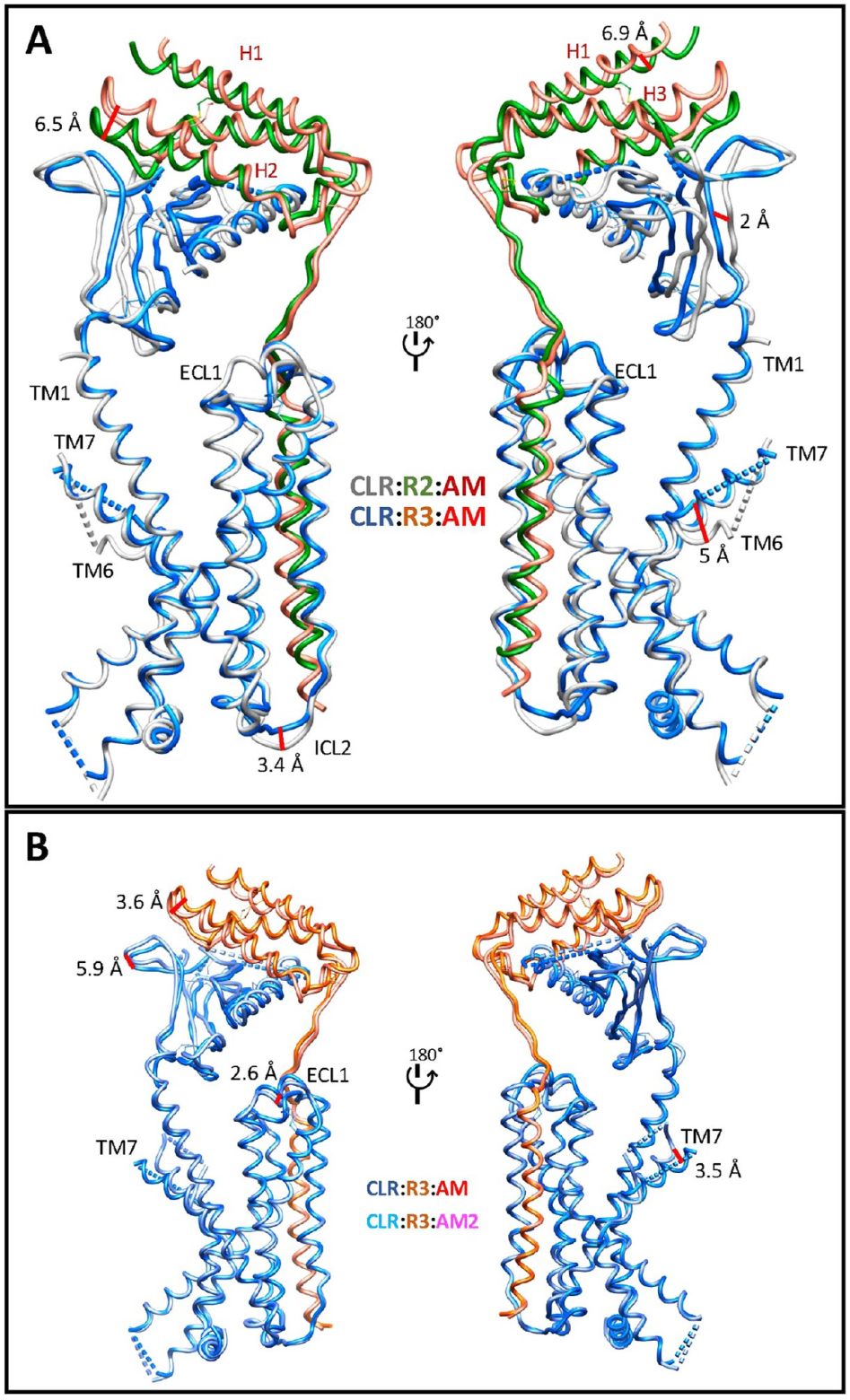

Figure 2. Overlay of the backbone structures in protein worm format of (A) the AM:AM$_1$R (CLR:R2:AM) and AM:AM$_2$R (CLR:R3:AM) complexes and (B) the AM:AM$_2$R and AM2:AM$_2$R (CLR:R3:AM2) complexes. The peptide and G proteins have been omitted for clarity. (A) RAMP2 and RAMP3 ECDs have different orientations relative to the CLR ECD, whereas (B) the difference in positioning of the ECD between the two AM$_2$Rs is due to a rigid body lateral movement. Distances in the TM domain in (A) are between the Cα of TM6 L351$^{6.55}$ (~5 Å) and ICL2 F246^{ICL2} (~3 Å) and in (B) are ECL1 V205^{ECL1} (2.6 Å) and TM7 V364$^{7.37}$ (2.6 Å). The CLR in the RAMP3 (R3) complexes is colored blue, and it is gray in the RAMP2 complex. RAMP2 is green, and RAMP3 is coral.

the AM$_2$R exhibited very similar backbone conformation for the transmembrane core of both CLR and RAMP3, with an ~3.5−6 Å lateral rigid body displacement of the CLR:RAMP3 ECD that propagated from a minor difference in the position of the extended TM1 helix (Figure 2B). Within the receptor core, there was a 2.6 Å shift in the position of ECL1

https://dx.doi.org/10.1021/acsptsci.9b00080
ACS Pharmacol. Transl. Sci. 2020, 3, 263−284

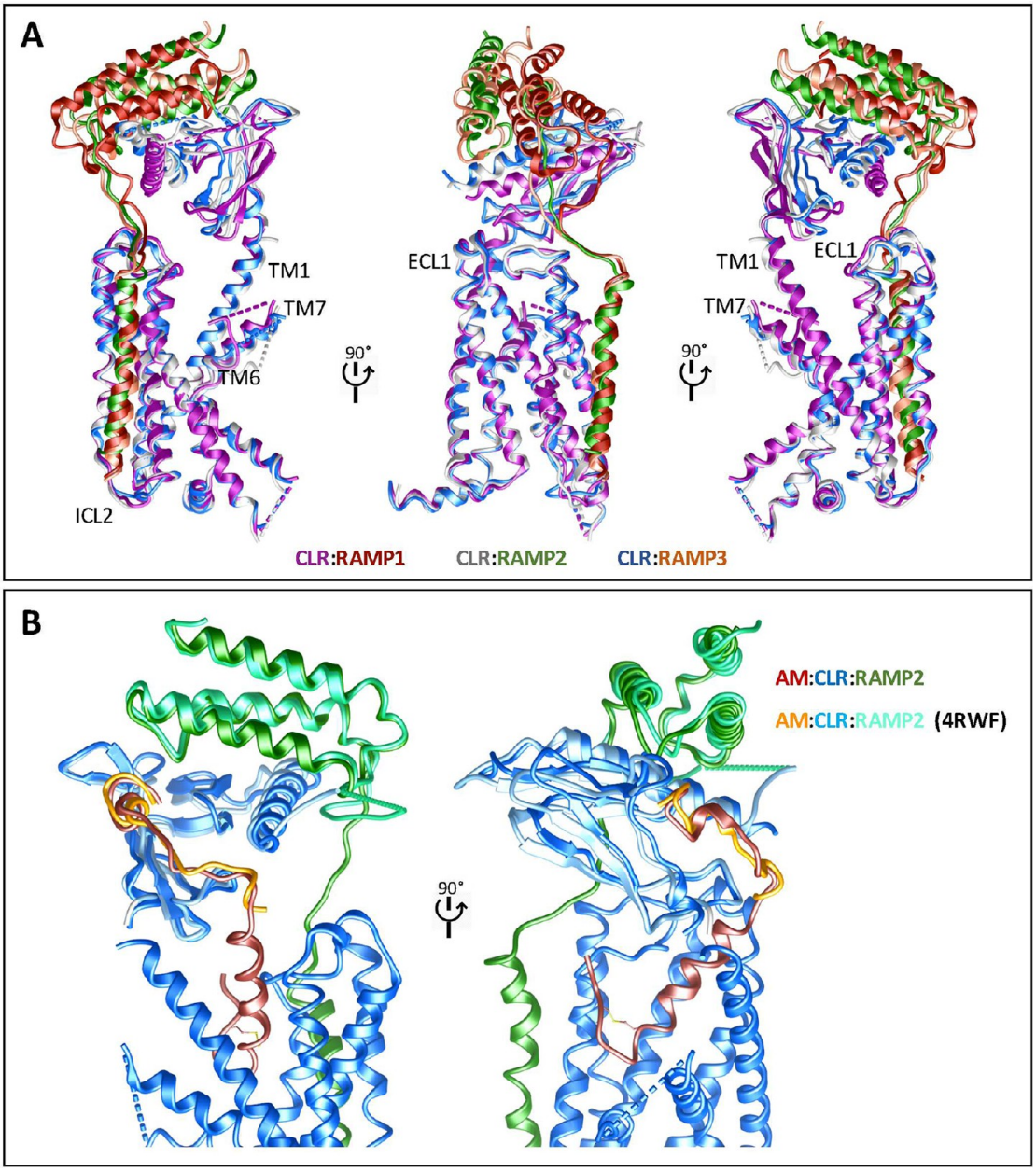

Figure 3. (A) Overlay of the backbone structures in ribbon format of the CGRP bound CGRPR (CLR:R1:CGRP), AM-bound AM_1R (CLR:R2:AM), and AM-bound AM_2R (CLR:R3:AM) complexes. CLR is colored as follows: in the CGRPR, dark pink, in the AM_1R, gray, and in the AM_2R, blue. RAMP1 is colored dark red, and RAMP2 is shown as green. RAMP3 is shown as coral. (B) Backbone (ribbon format) overlay of the AM:CLR:RAMP2 structure with the X-ray crystal structure of the ECDs of AM:CLR:RAMP2 (4RWF). Colors are as follows: cryo-EM structure: AM (red), CLR (blue), RAMP2 (green); 4RWF: AM (orange), CLR (light blue), RAMP2 (aquamarine).

(measured from the Cα of V205^{ECL1}), and distinctions in the location of the tops of TM6 and TM7, and by implication to the conformation of ECL3, although this was not resolved in the maps (Figure 2B). In contrast, there were greater differences in the receptor conformations of AM bound to the AM_1 and AM_2 receptors, respectively (Figure 2A). The most striking of these was in the orientation of the CLR ECD relative to either RAMP2 or RAMP3. In addition, there was a marked difference in the conformation of TM6 that was more kinked in the AM_1R (outwardly displaced by ~5 Å, measured from the Cα of L351$^{6.51}$; superscript corresponds to receptor amino acids are the conserved class B GPCR numbers; Figure 2A).[29] Prior mutagenesis studies have shown that there are differential impacts of several residues in this region on AM activity between the two receptors.[30]

At the intracellular face of the receptor, the largest difference observed was for ICL2 with a 3.4 Å displacement measured at the Cα of F246^{ECL2} (Figure 2A). The conformation of the transmembrane bundle of CLR in the CGRPR[20] most closely resembles that seen in the AM_1R, including the conformation of ICL2 and the angle of TM6 and TM7 at the extracellular face (Figure 3); however, the CLR:RAMP1 ECDs are more dramatically rotated compared to both AM receptors (Figure 3). This may contribute to the distinct peptide binding specificity of the CGRP receptor, although it is evident that the dynamic motion of the RAMPs and CLR play a key role in the allosteric modulation of

https://dx.doi.org/10.1021/acsptsci.9b00080
ACS Pharmacol. Transl. Sci. 2020, 3, 263−284

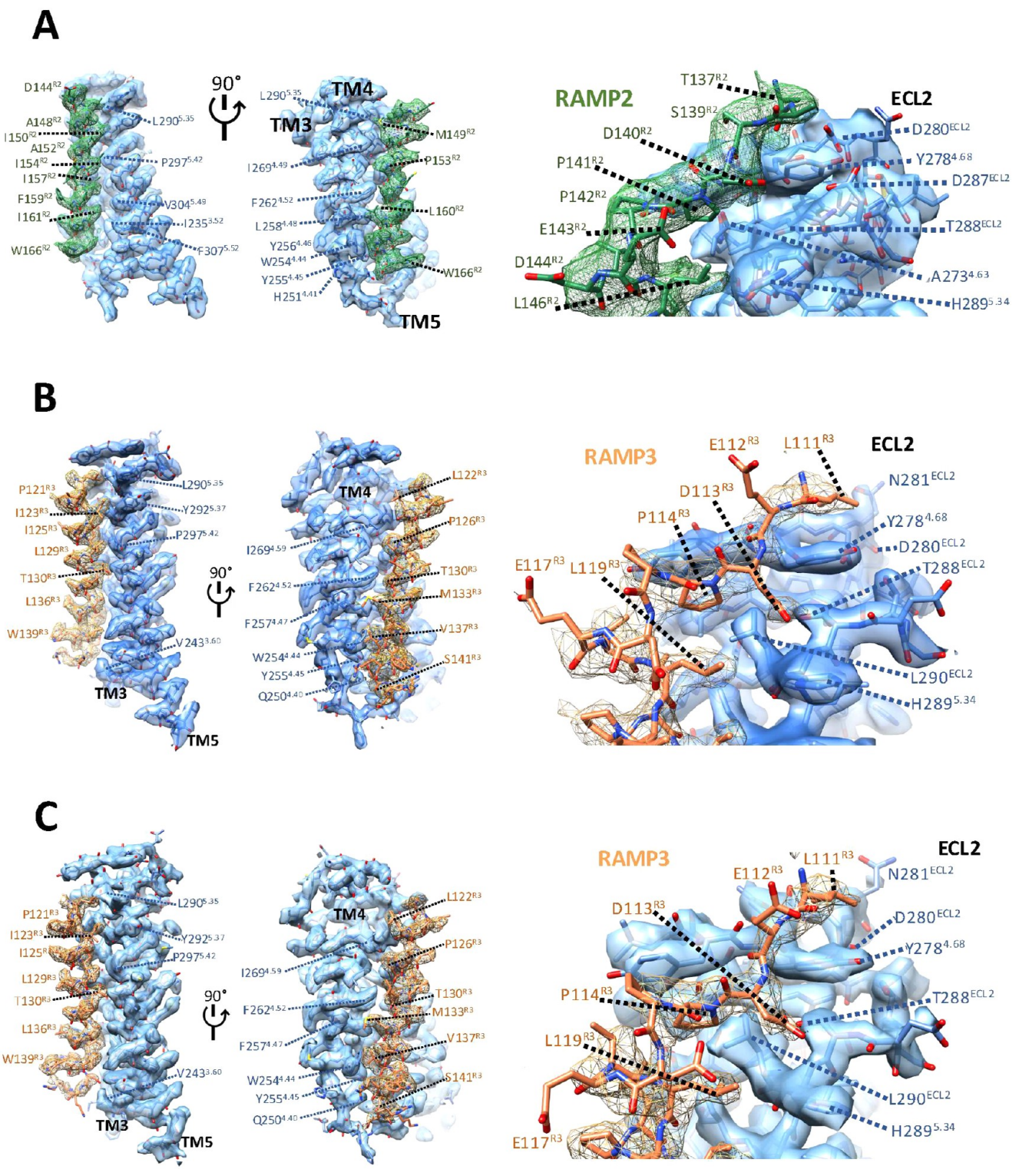

Figure 4. CLR-RAMP interface for the AM_AM$_1$R (A), AM_AM$_2$R (B), and AM2_AM$_2$R (C). Map to model figures illustrating tightness of TM packing (left panels), and extent of engagement of the proximal RAMP linker with ECL2 (right panel). Map density for the RAMP is shown as mesh. Map density for CLR is shown as a transparent surface. RAMP2 (green), RAMP3 (coral), and CLR (blue).

receptor phenotype by RAMPs (see below). We also compared the ECD of the AM-bound AM$_1$R to that of the equivalent structure of the isolated ECD domain solved by X-ray crystallography[21] (Figure 3B). While there was high similarity in the overall backbone conformation, when aligned to the CLR ECD, the RAMP2 ECD occupied a distinct position in the two structures. This is similar to the observation made for the CGRPR[20] and may reflect distinctions associated with the additional interactions that occur in the full-length, active receptor. Nonetheless, as noted below, the ECD is a highly dynamic domain in the cryo-EM structures.

RAMP−CLR Interface in AM Receptors. The surface charge of RAMP2 was predicted to be more acidic than that

https://dx.doi.org/10.1021/acsptsci.9b00080
ACS Pharmacol. Transl. Sci. 2020, 3, 263−284

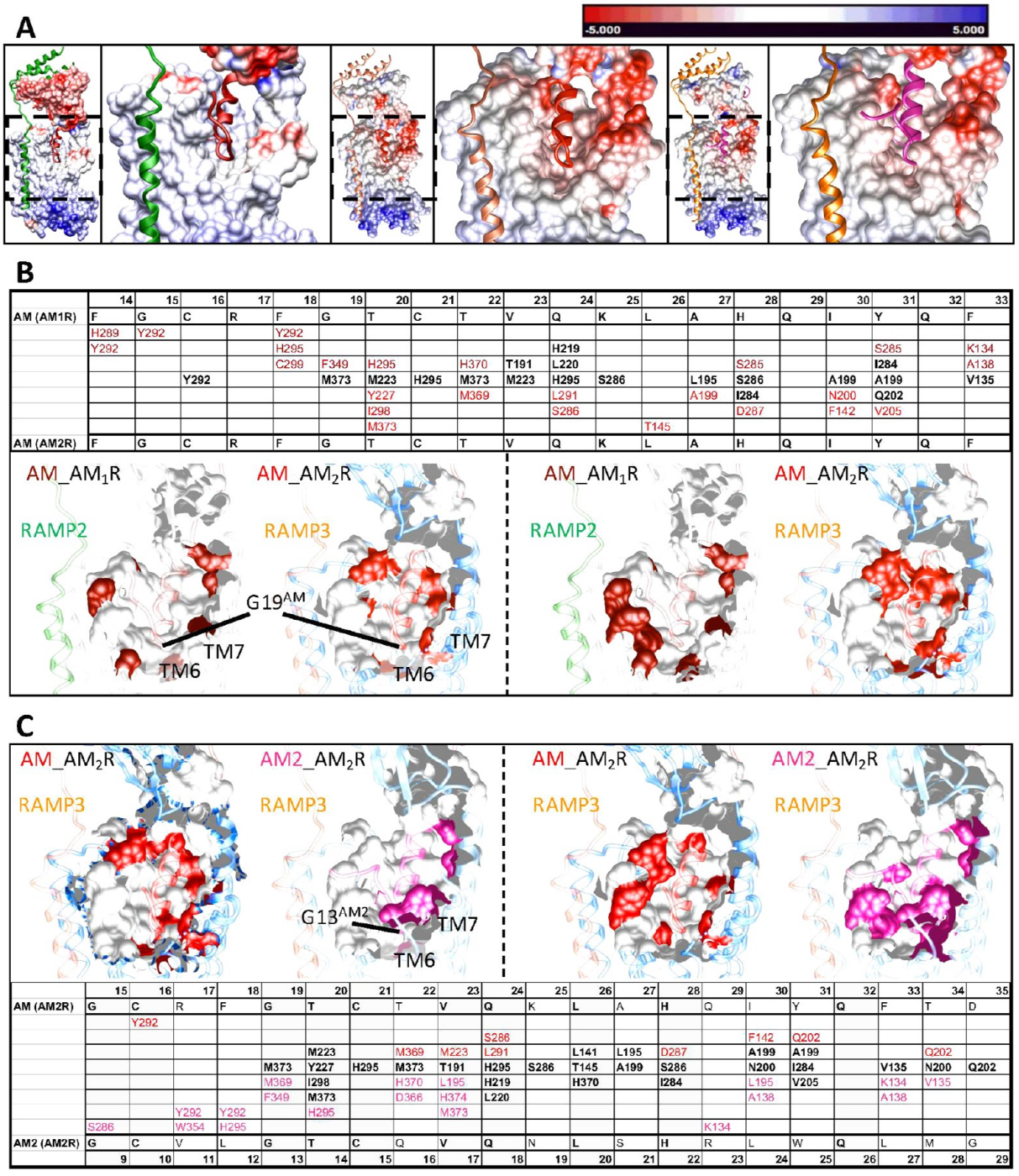

	14	15	16	17	18	19	20	21	22	23	24	25	26	27	28	29	30	31	32	33
AM (AM1R)	F	G	C	R	F	G	T	C	T	V	Q	K	L	A	H	Q	I	Y	Q	F
	H289	Y292			Y292															
	Y292				H295						H219							S285		K134
					C299	F349	H295		H370	T191	L220				S285			I284		A138
			Y292			M373	M223	H295	M373	M223	H295	S286		L195	S286		A199	A199		V135
							Y227		M369		L291			A199	I284		N200	Q202		
							I298				S286				D287		F142	V205		
							M373						T145							
AM (AM2R)	F	G	C	R	F	G	T	C	T	V	Q	K	L	A	H	Q	I	Y	Q	F

	15	16	17	18	19	20	21	22	23	24	25	26	27	28	29	30	31	32	33	34	35
AM (AM2R)	G	C	R	F	G	T	C	T	V	Q	K	L	A	H	Q	I	Y	Q	F	T	D
		Y292																			
										S286						F142	Q202				
						M223		M369	M223	L291		L141	L195	D287		A199	A199			Q202	
					M373	Y227	H295	M373	T191	H295	S286	T145	A199	S286		N200	I284		V135	N200	Q202
					M389	I298		H370	L195	H219		H370		I284		L195	V205		K134	V135	
					F349	M373		D366	H374	L220						A138			A138		
			Y292	Y292		H295			M373												
	S286		W354	H295											K134						
AM2 (AM2R)	G	C	V	L	G	T	C	Q	V	Q	N	L	S	H	R	L	W	Q	L	M	G
	9	10	11	12	13	14	15	16	17	18	19	20	21	22	23	24	25	26	27	28	29

Figure 5. AM and AM2 peptide binding to AM receptors. (A) Electrostatic surface potential for CLR for each of the receptor complexes (AM_1R ECD is from PDB: 4WRF), with the peptides and RAMPs shown as ribbon representation. Colors are as follows: in the AM_1R: AM (red) and RAMP2 (green); in the AM_2R: AM (dark red) and RAMP3 (light red); in the AM_2R: AM2 (dark pink) and RAMP3 (light pink). The electrostatic potential ranges from −5 (red) to +5 (blue) kT e^{-1}. (B) CLR residues selectively engaged (left panels) or differentially engaged (right panels) by equivalent amino acids of AM with the AM_1R and AM_2R, with common residues shown as gray surface representation and distinct interactions mapped in red (AM_AM_2R) or dark red (AM_AM_1R); specific interacting residues are detailed below. (C) CLR residues selectively engaged (left panels) or differentially engaged by (right panels) positionally equivalent amino acids of AM or AM2 with the AM_2R, with common residues shown as gray surface representation and distinct interactions mapped in red (AM_AM_2R) or dark pink (AM2_AM_2R); specific interacting residues are detailed below. The location of the deepest peptide residue in the binding pocket is highlighted ($G19^{AM}$; $G13^{AM2}$). For clarity in (B) and (C), CLR is colored differently; other colors are as follows: light gray, AM_AM_1R; blue, AM_AM_2R; light blue, AM2_AM_2R.

of RAMP3 (Figure S8A versus 8B,C), and the RAMPs formed extensive interactions with CLR between both the ECDs and TM domains. The former has previously been described for X-ray crystallography structures of the isolated ECDs of CLR and RAMPs.[21,28,31] Moreover, as observed in the full-length CGRPR,[20] interactions between RAMP and the peptide

https://dx.doi.org/10.1021/acsptsci.9b00080
ACS Pharmacol. Transl. Sci. 2020, 3, 263−284

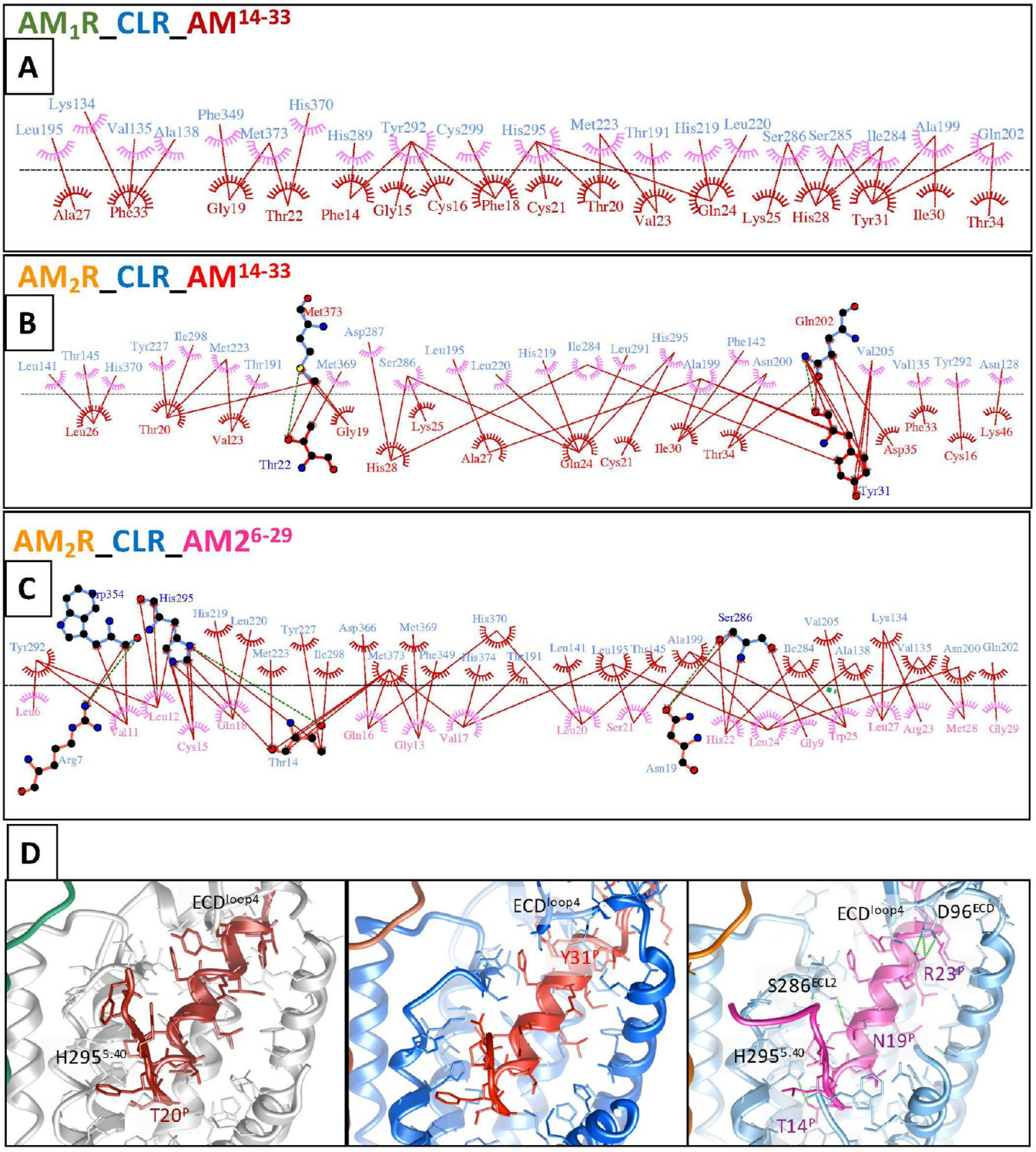

Figure 6. N-terminal peptide interactions with the TM core of CLR for the AM-bound AM_1R (A), AM-bound AM_2R (B), and AM2-bound AM_2R (C) calculated with using LigPlot+. Peptide residues are colored dark red (AM at AM_1R), red (AM at AM_2R), and dark pink (AM2 at AM_2R), and receptor residues are colored blue. Hydrophobic interactions are illustrated by red (AM) or pink (AM2) arcs with CLR in the reverse color, and interacting residues are joined by a red line. Amino acids involved in H-bonds are shown in atomic detail and H-bonds are shown as dashed green lines. (D) Structure models of N-terminal peptide binding to the AM_1R (left panel; AM, dark red; RAMP2, green; CLR, gray) or the AM_2R (middle panel: AM, red; RAMP3, coral; CLR, blue; right panel: AM2, dark pink; RAMP3, coral; CLR, light blue). The protein backbone is shown in a ribbon format, and side chains are shown in the x-stick format.

agonists were restricted to the far C-terminus of the peptides (Figure S8A−C).

Unsurprisingly, RAMP2 and RAMP3 interact with the equivalent transmembrane segments of CLR as observed for RAMP1,[20] forming an interface with TM3−5 (Figures 4A−C and S8A−F) and looping over ECL2 of CLR before forming a relatively disordered linker that connects the TMD to the RAMP ECD. Overall, RAMP3 exhibited tighter packing with

https://dx.doi.org/10.1021/acsptsci.9b00080
ACS Pharmacol. Transl. Sci. 2020, 3, 263−284

the CLR TMD compared with RAMP2 (Figure 4B,C versus 4A). While both RAMP2 and RAMP3 formed interactions with ECL2, the organization of the membrane proximal RAMP linker was distinct between the two RAMPs. In both AM and AM2 occupied structures, RAMP3 formed a H-bond between $D113^{R3}$ and both $T288^{ECL2}$ and $H289^{ECL2}$ (Figures 4B,C and S8E,F). The interaction with $T288^{ECL2}$ is also observed for RAMP1 and CLR in the CGRPR,[20] however, this was absent from RAMP2 despite conservation of the Asp residue, with no interaction of the positionally equivalent $D140^{R2}$ with ECL2 of CLR (Figures 4A and S8D). However, a potential H-bond occurring between $S139^{R2}$ and $T288^{ECL2}$ may also limit productive engagement with ECL2 (Figures 4A and S8D).

Peptide Binding to AM Receptors. Density for AM peptide and receptor in the ECD in AM_1R, and the overall density of both RAMP2 and RAMP3 ECD in all structures was limited. As such, we concentrated our analysis on the engagement of the peptide N-terminus with the receptor core that drives receptor activation. AM and AM2 have extended N-termini, relative to CGRP, but these residues are not required for functional activity of the peptides.[29,32,33]

Similar to the CGRPR,[20] there were no direct interactions between the peptide N-termini and the RAMPs (Figures 5 and 6). All peptides adopted a similar conformation consisting of an N-terminal loop formed by a conserved disulfide bridge ($C16^{AM}$–$C21^{AM}$; $C10^{AM2}$–$C15^{AM2}$) followed by a short amphipathic α-helix that terminated where the peptides exited the TM core of the receptors ($C21^{AM}$–$F33^{AM}$; $C15^{AM2}$–$Q26^{AM2}$) (Figures 5B,C and 6D). The structure of the loop was further reinforced by likely H-bonds between backbone of $C10^{AM2}$/$C16^{AM}$ and the side chain of $N19^{AM2}$ or $K25^{AM}$. Substitution of $K25^{AM}$ with Ala results in modest effects on signaling.[33] The far N-terminus of the peptides exited away from the surface of the receptor, providing a structural explanation for the lack of functional importance of the extended N-termini of AM and AM2.

The deepest residue in the receptor core was the conserved Gly, $G13^{AM2}$/$G19^{AM}$ (Figure 5B,C). Substitution of $G19^{AM}$ with Ala has profound effects on activity in a pathway-specific manner,[33] while substitution of $G13^{AM2}$ with Ala has marked effects on peptide potency.[32] In all cases, the peptides bind into an open cavity that is enabled by the splayed outward movement of TM6/TM7/ECL3, and there are limited interactions between the peptides and this segment of the receptors (Figure 5A). Despite all interactions between the peptide and receptors in the receptor core occurring with the common CLR subunit, the binding pocket for the AM_2R presented a more acidic environment than that of the AM_1R, albeit that this was partially influenced by the bound peptide (Figure 5A).

Unsurprisingly, the overall pattern of peptide interaction for the two AM receptors was similar, with interactions principally with TM3, TM5, and ECL2, with additional interactions toward the top of TM2 and TM1 (Figures 5B,C and 6). These included key conserved interactions observed across other class B GPCRs,[23] such as with positions 1.33, 1.36, 2.64, 2.68, 3.36, 3.37, 3.44, and 5.40. For the latter, $H295^{5.40}$ in CLR, this formed a H-bond with $T14^{AM2}$ in the AM_2 receptor, while it likely forms transient H-bonds with $T20^{AM}$ at AM_1R and AM_2R. CLR mutagenesis studies support this role of $H295^{5.40}$, and substitution of $T20^{AM}$ with Ala substantially reduces peptide activity.[33] Similarly, a loss of peptide potency has been observed in prior investigation[32] of $T14^{AM2}$. As previously noted,[23] mutation of 5.40 in class B GPCRs leads to attenuation of signaling, indicative of a key role in driving G protein coupling.[26,33−37] Interestingly, for AM binding to the AM_1R there are more selective interaction or distinct types of interactions with the distal segment of ECL2 compared with AM_2R interactions, where there were more selective interactions with the middle region of ECL2 and adjacent residues that line the binding site as the peptide exits the TM core (Figure 5B). Comparison of the interactions between AM and AM2 with the AM_2R revealed that AM2 made more extensive interactions than AM, with positionally equivalent amino acids, perhaps not surprisingly, forming distinct interaction patterns with residues in TM1, TM7, and ECL2 (Figures 5C, right panels, and 6B,C), although there were more selective residue interactions observed for AM (Figure 5C, left panels). $N19^{AM2}$ forms a H-bond with $S286^{ECL2}$ and this may increase stability of AM2 binding in the AM_2R, despite generally greater specific interactions between AM and ECL2 in this receptor (Figures 5C and 6B,C). Interestingly, the interactions of AM, AM2, and CGRP[20] with ECL2 occur principally at the mid-distal (TM5) end of the helix, similar to what is also observed for the related CTR but distinct from other class B GPCRs that bind peptides with extended helices. In those receptors, the interactions are greater with more proximal ECL2 residues, and this distinction may, in part, explain the large differences in the effect of Ala mutations of ECL2 on peptide efficacy seen between GLP-1R and CTR,[38−40] which can be further modified by RAMP interaction.[41]

The lateral displacement of TM1 and the ECD in the AM2:AM_2R leads to the fourth loop of the CLR ECD being located closer to the AM2 peptide as it exits the receptor, compared with AM at either the AM_1R or AM_2R (Figure 6D). In the AM2:AM_2R complex, there is extensive H-bonding between $R23^{AM2}$ and $D96^{ECD}$ and the potential for additional transient H-bonds with $S98^{ECD}$ (Figure 6D), and this may influence the relative positioning of the ECDs relative to the receptor core.

In general, there were more differential interactions between AM binding to the AM_2R rather than at the AM_1R and for AM2 compared with AM binding to the AM_2R (Figure 5B,C). The latter differences are likely due to the divergence in more C-terminal residues of the peptide helices between AM and AM2, leading to distinct interactions of AM2 with TM1 and the ECD as the peptide exits the receptor core (Figures 5B,C and 6). This may, in part, contribute to the greater potency of AM2 at the AM_2R relative to AM_1R.[5] Collectively, the observed interactions in the structures are generally consistent with the known structure−function relationships for AM peptides binding to AM receptors,[30,32,33,37,42] with exceptions likely related to dynamics of binding to the receptor, including entry to and egress from the receptor core.

Unlike other active-class B GPCR structures, including the CGRPR,[20,23] there is very limited interaction between the peptides and TM7 of the AM receptors. In other class B GPCRs, it has been postulated that peptide-specific interactions with TM7/ECL3/TM6 may be involved in biased agonism that has been described at these receptors.[43] The functional significance of the current observations is unclear; however, little biased agonism is seen at the AM receptors,[33] consistent with interactions with TM7/ECL3/

https://dx.doi.org/10.1021/acsptsci.9b00080
ACS Pharmacol. Transl. Sci. 2020, 3, 263−284

TM6 being drivers for biased agonism, at least for class B GPCRs.

Receptor−G Protein Interface. The conformation of the receptor at the interface with the G protein was very similar for all three structures, with the exception of ICL2 that adopted a distinct conformation in a RAMP-dependent manner (Figure 7A−C). Not surprisingly, the overall interface

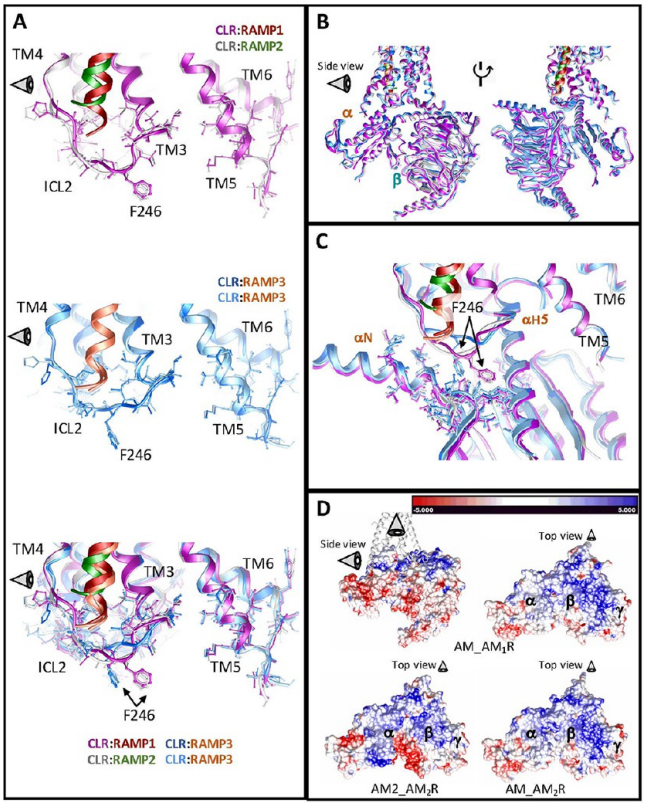

Figure 7. Comparison of the receptor:G protein interface across CLR:RAMP receptor heterodimers. (A) Overlay of the intracellular face of the CGRP and AM_1 receptors, highlighting the common positioning of most side chains. The largest exception was in the position of F246 in ICL2 that occupied a common position between the CGRPR and AM_1R (upper panel), as well as between the different peptide-bound AM_2R (middle panel), but was distinct between AM_2R and the other receptors (lower panel). (B) The G protein occupies a common global interaction position that is highly similar in conformation across receptors. (C) Close up of panel B, boxed area, focusing on the interaction with ICL2. (D) The bound Gs heterotrimer has a similar surface electrostatic potential when binding to AM receptors. The protein backbone is shown in a ribbon format, and side chains are shown in the x-stick format. RAMP1 is colored dark red, RAMP2, green, RAMP3, coral. CLR in the CGRPR is colored dark pink, in the AM-bound AM_1R, gray, in the AM-bound AM_2R, blue, in the AM2-bound AM_2R, light blue. G proteins are colored equivalent to CLR for each receptor.

of the G protein with the receptor was nearly identical (Figure 7D), with the G proteins virtually overlaid across both the AM receptors and the previously published CGRPR[20] (Figure 7B). Within ICL2, the largest difference was in the location of $F246^{ICL2}$ that was deeper in the groove between the Gαs αN and αH5 helices for the AM_1R, compared to the AM_2R, regardless of bound peptide. Interestingly, the position of $F246^{ICL2}$ in the CGRPR was equivalent to that of the AM_1R (Figure 7A,C). The specific interactions of the C-terminal end of the Gs αH5 that extends into the receptor cavity were highly conserved across the three structures, particularly for the last 5 amino acids (Figures 7C and 8C). However, there were differences in engagement of the Gs αN arising from the distinct ICL2 conformation (Figures 7 and 8). In the complexes, the G protein−receptor interaction is stabilized by mutations to the α-subunit[20,24,25] and Nb35, a prerequisite to stable complex formation and structure determination. Nonetheless, this may contribute to the similarity in observed interactions in the current structures. The CLR-based receptors also interact with an additional, intracellular accessory protein, CGRP Receptor Component Protein (RCP), and this interaction is important for efficiency of Gs signaling by CGRP and AM receptors.[44] The site of RCP interaction with CLR is reported to be ICL2.[45] As such, RAMP-dependent differences in the conformation of CLR ICL2 could influence RCP engagement and Gs signaling.

RAMPs Allosterically Alter CLR Conformational Dynamics to Engender CGRP and AM Receptor Phenotype. One of the most fundamental questions for RAMP-complexed GPCRs is what is the mechanistic basis for RAMP modulation of receptor phenotype? This has been particularly puzzling as the RAMPs form only very limited direct interaction with the far C-terminus of the peptides, and substitution of the C-terminal peptide residues does not lead to substantially altered receptor specificity.[21] Likewise, structural and biochemical studies of the isolated ECDs of CGRP and AM_1 and AM_2 receptors have not provided clues as to the major determinant(s) for the altered receptor phenotypes, despite identification of important ECD residues for peptide interactions.[21,28,31,42,46] The current AM receptor structures, together with our previously published structure of the CGRPR, has enabled consideration of the differences that occur across the three RAMP modulated receptors in their peptide-bound activated states. Somewhat surprisingly, with the exception of TM7/ECL3/TM6 that do not directly contact the peptides, the packing of the transmembrane core and the interactions made by the peptide N-terminal domain with the core were remarkably similar in the consensus structures. This suggests that conformational dynamics of the RAMP−CLR complexes, rather than the consensus metastable interactions, may be the principal drivers of distinct receptor phenotypes. The largest difference in the structures was in the location of the ECDs, relative to the receptor core (Figures 2 and 3), with the location of the ECDs in the CGRPR more distinct from the AM receptors than the differential location of the ECDs between AM_1R and AM_2R. Previous molecular dynamics (MD) simulations of the CGRPR in the presence and absence of RAMP1 indicated that the presence of the RAMP limits the dynamic motion of the CLR ECD,[20] consistent with the notion that the RAMP influence on receptor dynamics could underpin differences in observed functional phenotype.

Unlike X-ray crystallography, a potential advantage of cryo-EM is the ability to observe dynamics of the protein complexes as distinct conformations captured during sample vitrification.[47,48] The lower resolution of the ECDs in the consensus maps suggested that such dynamic information was present in the current cryo-EM data, and the large number of particles and high relative resolution of the data provided a potential opportunity to understand relative motions of the different AM receptor complexes. 3D multivariate analysis in cryoSPARC was applied to the AM receptor data, as outlined

https://dx.doi.org/10.1021/acsptsci.9b00080
ACS Pharmacol. Transl. Sci. 2020, 3, 263−284

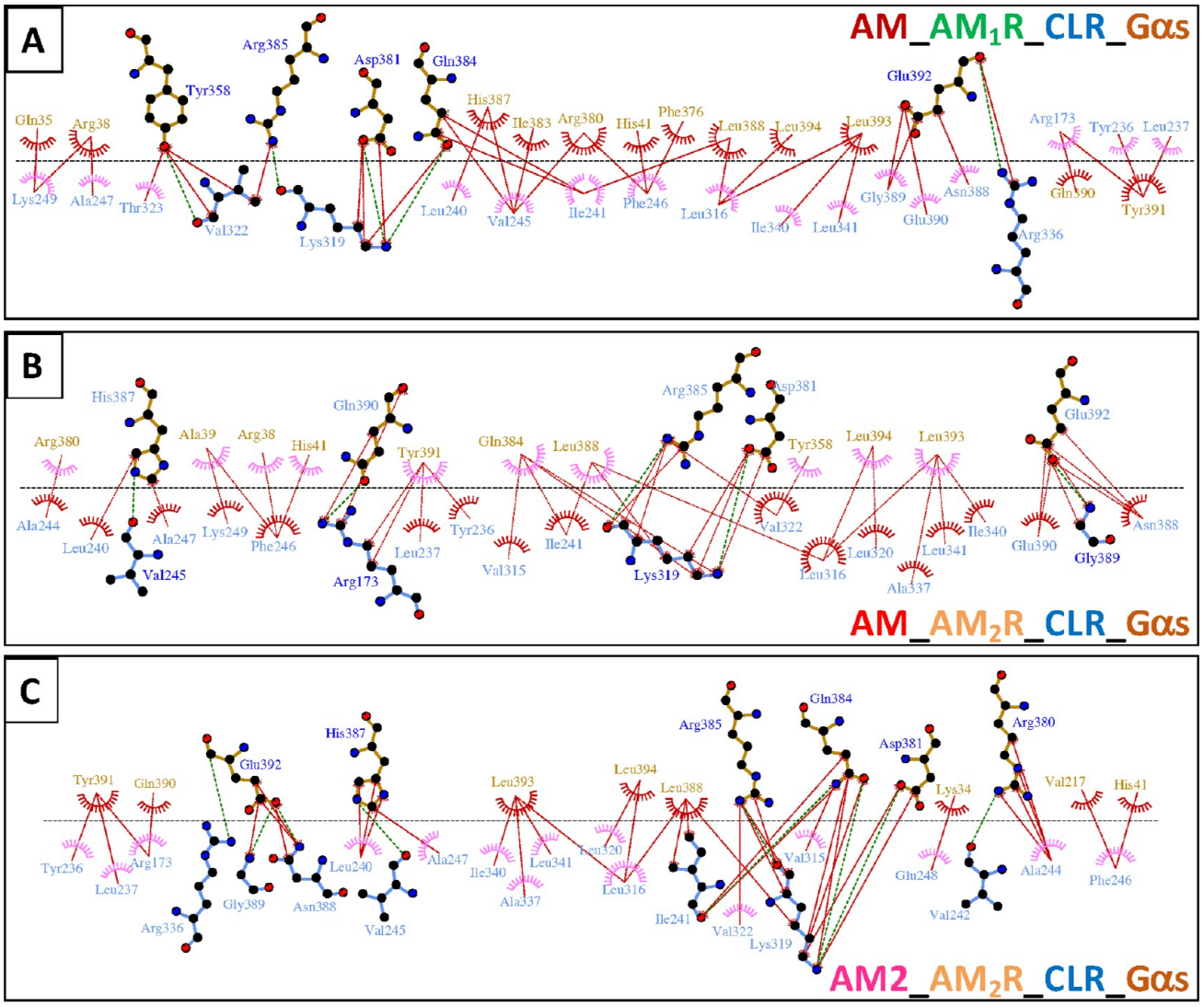

D

Gαs_αN ← → Gαs_αH5

Gs_alpha	K34	Q35			R38	A39		H41		V217		Y358		F376				R380	D381		I383	Q384	R385		H387	L388		Q390	Y391	E392	L393	L394
AM_AM1R		K249			A247			F246				V322		F246				V245	K319		V245	I241	K319		L240	I241		R173	R173	R336	L316	L316
					K249							T323						F246				V245	V322		V245	L316			Y236	N388	I340	
																						K319							L237	G389	L341	
																														E390		
AM_AM2R					F246	F246		F246				V322						A244	K319			I241	K319		L240	L316		R173	R173	N388	L316	L316
						K249																V315	V322		V245	K319			Y236	G389	A337	L320
																						K319			A247				Y237	E390	I340	
																															L341	
AM2_AM2R	E248							F246		F246								V242	K319			I241	K319		L240	I241		R173	R173	R336	L316	L316
																		A244				V315	V322		V245	L316			Y236	N388	A337	L320
																						K319			A247	K319			Y237	G389	I340	
																															L341	

Figure 8. CLR−Gαs interface for AM_AM$_1$R (A), AM_AM$_2$R (B), and AM2_AM$_2$R (C). Interactions were determined using LigPlot+. Gαs residues are gold, and receptor residues are blue. Hydrophobic interactions are illustrated by red or pink arcs adjacent to residue labels, and interacting residues are joined by a red line. Amino acids involved in H-bonds are shown in atomic detail with H-bonds shown as dashed green lines. (D) Summary of the specific interactions. Interactions common to all 3 receptor complexes are shown in bold and are shaded light green. Residues involved in H-bond interactions are shown in green type. Interactions common to AM bound to AM$_1$R and AM$_2$R only are shaded light orange. Interactions common to complexes of the AM$_2$R only are shaded yellow. Interactions common to AM bound to AM$_1$R and AM2 bound to AM$_2$R only are shaded blue.

in Figure S9. This analysis has the potential to separate global motions that can be grouped via principal components. As such, this can provide insight into the coordinated motion of the complexes. For all receptors data was partitioned into 3 normal modes (Movies S1−S3, S6−S8, and S11−S13), and this analysis indicated that a component of the motions of the ECDs and G protein occur in a coordinated manner, suggesting that the breadth of ECD motion may be partially linked to conformational dynamics of the receptor-G protein interface (and vice versa). While the quality of the data for the

https://dx.doi.org/10.1021/acsptsci.9b00080
ACS Pharmacol. Transl. Sci. 2020, 3, 263−284

AM_1R complex with AM created additional noise relative to the AM_2R complexes, the analysis revealed that the AM_1R had greater overall motion (Movies S1−S3) than the corresponding AM_2Rs (Movies S6−S8 and S11−S13), and this was particularly reflected in the dynamics of the ECD, and is consistent with the lower resolution of this domain for AM_1R in the consensus map (Figure 1B). As noted above for the consensus map, the RAMP3 TM has tighter packing interactions with the receptor TM and stronger interactions between the proximal linker domain and the receptor ECL2. This limits the motion of the RAMP3 and maintains interactions with ECL2 across the observed sub conformations (Figure 9B,C; Movies S9 and S14). In contrast, the

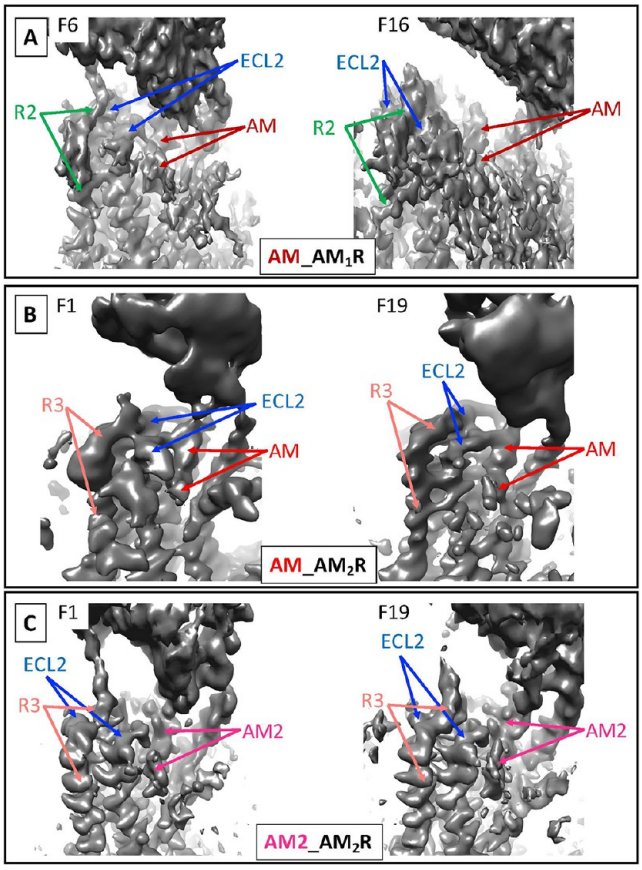

Figure 9. cryoSPARC multivariate analysis of the AM-bound AM_1R (A), AM-bound AM_2R (B), and AM2-bound AM_2R (C) focusing on the interface of the RAMP and ECL2. Three normal modes were captured as 20 map files for each receptor complex and snapshots of the first and last frame (F1 and F19, respectively) are displayed for the AM_2R complexes (B, C). For AM_1R, due to the greater noise in the data, the early and late frames primarily reflected loss of signal; as such, F6 and F16, which represent the ends of the motion, are displayed (A). Map density is displayed as a gray surface.

weaker interactions of RAMP2 appear to lead to almost complete disengagement of the proximal linker with ECL2 and the much broader motions of the ECD noted above (Figure 9A; Movie S4), with the AM peptide also appearing to make more transient interactions with the receptor core than either of the peptides with the AM_2R, although the resolution of the AM_1R complex does not allow for this to be analyzed at a molecular level.

A second interesting observation from the dynamic conformational analysis was revelation that the RAMP3 C-terminus made transient interactions with the G protein αN helix for both AM2 and AM-bound complexes (Figure 10B,C;

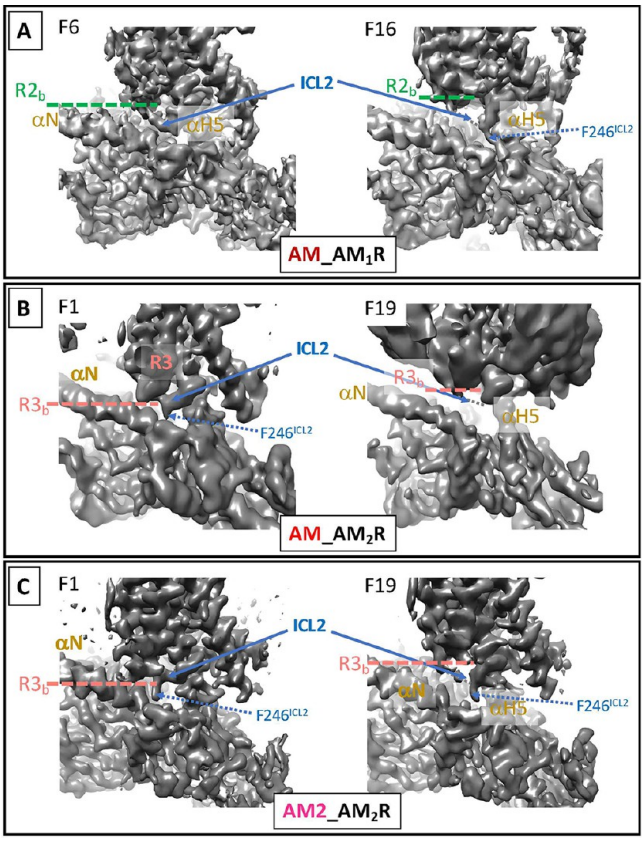

Figure 10. cryoSPARC multivariate analysis of the AM-bound AM_1R (A), AM-bound AM_2R (B), and AM2-bound AM_2R (C) focusing on the interface of Gαs and the receptors, particularly the RAMP C-terminus and ICL2. Three normal modes were captured as 20 map files for each receptor complex and snapshots of the first and last frame (F1 and F19, respectively) are displayed for the AM_2R complexes (B, C). For the AM_1R, due to the greater noise in the data, the early and late frames primarily reflected loss of signal; as such, F6 and F16, which represent the ends of the motion, are displayed (A). Map density is displayed as a gray surface. Color key: CLR, blue; RAMP2, green; RAMP3, coral; Gαs, gold. The end of the resolved density for each of the RAMPs is illustrated with a dashed line labeled with R2b (RAMP2) or R3b (RAMP3).

Movies S10 and S15), although this was more evident in the AM2:AM_2R data. However, this was not observed for the RAMP2 complex (Figure 10A; Movie S5) and may contribute to the differences in the metastable ICL2 conformation noted in the consensus structures, although the functional importance of this is currently unclear. This may be linked to the conformational sampling of ICL2 as the extension to the base of RAMP3 appeared to be correlated with strength of the density for $F246^{ICL2}$ in the consensus map position for the AM_2R structures (Figure 10B,C; Movies S10 and S15).

As the multivariate analysis could not be applied to the CGRPR (RAMP1) data, we performed MD simulations on the CGRPR complex in comparison to equivalent simulations on the AM_1R complex (Movie S16). Consistent with the observations in analysis of the cryo-EM data, in the simulations RAMP2 formed transient interactions with

https://dx.doi.org/10.1021/acsptsci.9b00080
ACS Pharmacol. Transl. Sci. 2020, 3, 263−284

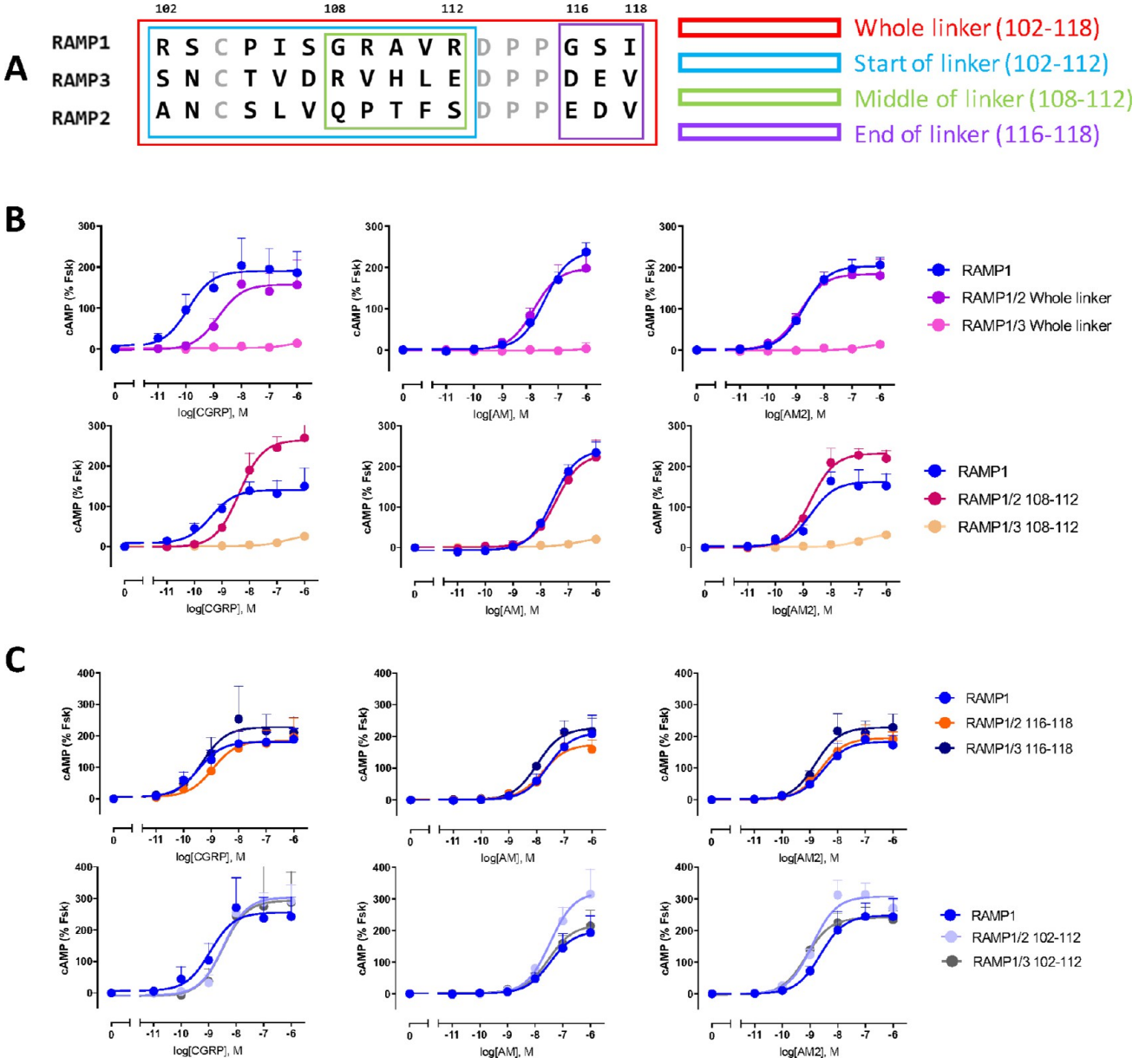

Figure 11. Pharmacological analysis of RAMP1 linker chimeras with RAMP2 or RAMP3. (A) Amino acid sequence of the linker regions (numbered using the RAMP1 sequence for simplicity), with the different length chimeras denoted by colored boxes: red, whole linker (102−118); blue, N-terminal linker region (102−112); green, mid-linker region (108−112); purple, C-terminal linker region (116−118). Conserved residues are in gray, and divergent residues are in black. (B, C) Peptide concentration−response was measured in cAMP accumulation assay, following transient expression of constructs into COS-7 cells, for full linker exchange (B, upper panel) or exchange of the 108−112 segment (B, lower panel), the 116−118 segment (C, upper panel), or the 102−112 segment (C, lower panel).

ECL2, and this was paralleled by relatively transient interactions of the more distal segment of the linker with the CLR ECD, giving rise to broad motions of the ECD relative to the receptor core. In contrast, the proximal RAMP1 linker formed much more stable interaction with ECL2, and this was also true of the distal linker with the CLR ECD, giving rise to both the distinct orientation seen in the cryo-EM structure and much more limited mobility of the ECD domain. We also extended the analysis of the AM_1R using principal component analysis (Movies S17 and S18−S22), and this revealed similar patterns of coordinated motions between the receptor and G protein to those observed in the different normal modes of the 3D multivariate analysis of the cryo-EM data, providing additional support for the notion of coordinated motion between the receptor ECD and G protein (Movies S17 and S20−S22).

Membrane-Proximal RAMP Linker Region Is Critical in AM Receptor Dynamics and Functional Phenotype. The multivariate analysis described above revealed greater dynamic motion of the AM_1R relative to the AM_2Rs, including movement of the membrane proximal RAMP2 linker away from ECL2 and destabilization of the AM binding pose that is likely associated with the weaker interactions observed in the static structure. As such, we postulated that this domain may be a key contributor to the allosteric regulation of CLR phenotype by RAMPs and consequently generated a series of chimeras between the three RAMPs, exchanging different segments of the linkers (summarized in Figure 11A; Table 1).

https://dx.doi.org/10.1021/acsptsci.9b00080
ACS Pharmacol. Transl. Sci. 2020, 3, 263−284

Table 1. Summary of pEC_{50} and E_{max} Values for cAMP Production at CLR + RAMPs or RAMP Chimera Constructs in Cos7 Cells Stimulated with CGRP, AM, or AM2[a]

	CGRP		AM		AM2	
	pEC_{50}	E_{max}	pEC_{50}	E_{max}	pEC_{50}	E_{max}
			RAMP1 Whole Linker			
RAMP1	9.96 ± 0.42 (3)	190 ± 21	7.48 ± 0.11 (5)	239 ± 12	8.72 ± 0.13 (5)	203 ± 6
RAMP1/2	8.84 ± 0.37 (3)[c]	157 ± 20	7.86 ± 0.20 (5)	197 ± 18	8.86 ± 0.24 (5)	184 ± 14
RAMP1/3	N.D.	N.D.	N.D.	N.D.	N.D.	N.D.
			RAMP1 102−112			
RAMP1	8.95 ± 0.40 (3)	256 ± 33	7.45 ± 0.30 (4)	199 ± 28	8.62 ± 0.28 (4)	248 ± 23
RAMP1/2	8.47 ± 0.17 (3)	304 ± 18	7.46 ± 0.23 (4)	321 ± 34[b]	8.92 ± 0.17 (4)	308 ± 17
RAMP1/3	8.49 ± 0.48 (3)	294 ± 51	7.50 ± 0.21 (4)	217 ± 21	9.13 ± 0.14 (4)	241 ± 11
			RAMP1 108−112			
RAMP1	9.40 ± 0.35 (5)	141 ± 13	7.57 ± 0.12 (5)	241 ± 13	8.72 ± 0.27 (5)	162 ± 14
RAMP1/2	8.38 ± 0.19 (4)[c]	265 ± 18[b]	7.45 ± 0.16 (4)	230 ± 17	8.73 ± 0.14 (4)	232 ± 11[b]
RAMP1/3	N.D.	N.D.	N.D.	N.D.	N.D.	N.D.
			RAMP1 116−118			
RAMP1	9.46 ± 0.31 (4)	181 ± 15	7.58 ± 0.31 (4)	213 ± 29	8.52 ± 0.23 (4)	183 ± 14
RAMP1/2	8.94 ± 0.38 (4)	185 ± 22	7.78 ± 0.22 (4)	175 ± 16	8.60 ± 0.22 (4)	195 ± 15
RAMP1/3	9.32 ± 0.45 (4)	228 ± 30	7.97 ± 0.17 (4)	227 ± 16	8.79 ± 0.25 (4)	229 ± 19
			RAMP2 Whole Linker			
RAMP2	7.06 ± 0.13 (3)	101 ± 7	9.59 ± 0.36 (5)	78 ± 8	8.50 ± 0.20 (5)	97 ± 7
RAMP2/1	6.93 ± 0.25 (3)	205 ± 31[b]	9.77 ± 0.49 (5)	162 ± 20[b]	8.16 ± 0.30 (5)	163 ± 20[b]
RAMP2/3	7.20 ± 0.07 (3)	142 ± 5	9.12 ± 0.35 (5)	202 ± 23[b]	9.05 ± 0.23 (5)	162 ± 12[b]
			RAMP2 Shorter Chimera			
RAMP2	N.D.	N.D.	9.51 ± 0.18 (8)	97 ± 5	8.73 ± 0.17 (8)	99 ± 6
RAMP2/3 102−112	N.D.	N.D.	9.81 ± 0.28 (4)	75 ± 6	9.00 ± 0.31 (4)	83 ± 8
RAMP2/3 108−112	N.D.	N.D.	9.77 ± 0.54 (3)	82 ± 12	8.20 ± 0.30 (3)	92 ± 11
RAMP2/3 116−118	N.D.	N.D.	9.70 ± 0.28 (4)	92 ± 7	8.82 ± 0.30 (4)	109 ± 11
			RAMP3 Whole Linker			
RAMP3	6.96 ± 0.20 (4)	159 ± 19	9.38 ± 0.37 (5)	107 ± 12	9.34 ± 0.16 (5)	120 ± 6
RAMP3/1	7.08 ± 0.19 (4)	177 ± 18	9.17 ± 0.18 (5)	160 ± 9[c]	9.33 ± 0.16 (5)	159 ± 8[b]
RAMP3/2	7.16 ± 0.31 (4)	93 ± 15	10.46 ± 0.74 (5)	98 ± 17	8.96 ± 0.32 (5)	101 ± 11
			RAMP3 Shorter Chimera			
RAMP3	N.D.	N.D.	9.61 ± 0.38 (8)	138 ± 13	9.59 ± 0.30 (8)	149 ± 12
RAMP3/2 102−112	N.D.	N.D.	9.10 ± 0.26 (4)	138 ± 10	9.00 ± 0.44 (4)	128 ± 18
RAMP3/2 108−112	N.D.	N.D.	9.36 ± 0.17 (4)	146 ± 7	9.41 ± 0.13 (4)	165 ± 6
RAMP3/2 116−118	N.D.	N.D.	9.60 ± 0.27 (4)	136 ± 10	9.50 ± 0.35 (4)	115 ± 11

[a]Values are mean ± SEM from 3 to 8 individual experiments performed in triplicate. Numbers of individual experiments are in brackets. E_{max} values are normalized to the response with 100 μM forskolin. N.D. is used when no curve could be fit to the data. Separate control (wild-type) RAMPs were used for each batch of chimeric RAMPs. [b]Significantly different from parental construct at 95% confidence intervals. [c]Significantly different from parental construct by *F*-test of fitted value at $P < 0.05$.

These were studied in assays of receptor expression and cAMP accumulation (Figures 11, 12, and S10). Most of the chimeras retained the ability to traffic with CLR to the cell surface, with the exceptions being exchange of RAMP1 for the full linker (102−118) or mid-linker region (108−112) of RAMP3 that were poorly expressed and could not be characterized (Figure S10). For simplicity, the numbering for all exchanges is that of the linker in the RAMP1 peptide (Figure 11A).

RAMP1 Linker Exchange. Exchange of the RAMP1 linker with the whole RAMP2 linker, or the shorter 108−112 in each case led to loss of CGRP potency, while there was a smaller attenuation of potency for the 116−118 fragment that did not achieve significance (Figures 11B,C, Table 1). Intriguingly, for the 108−112 chimera, this was also accompanied by enhanced E_{max}. This latter observation may be consistent with the correlated dynamics of the ECDs and G protein observed in the analysis of conformational dynamics described above whereby changes to mobility of the RAMP1 ECD with the chimeras may also alter efficiency of G protein turnover, which is linked to ligand efficacy.[49] There was only relatively limited impact of the exchanges on AM potency but enhanced E_{max} of AM2 was observed for the 108−112 RAMP1/2 chimera (Figure 11B, Table 1).

RAMP2 Linker Exchange. Full RAMP2 linker exchange with either that of either RAMP1 or RAMP3 had substantive effects on AM and AM2 responses. For AM or AM2, the response E_{max} was increased with either exchange (Figure 12A; Table 1), and potency was also increased for AM2 with the RAMP3 exchange, albeit that this did not achieve statistical significance (Figure 12A; Table 1). For CGRP, an increased response was observed with both chimeras but the potency was too low to robustly quantify (Figure 12A). Shorter chimeras with RAMP3 had minimal effect on AM or AM2 responses (Figure 12A; Table 1).

RAMP3 Linker Exchange. Full linker exchange with RAMP1 induced only small increases in both AM and AM2 peptide E_{max}. The exchange with RAMP2 also led to an

https://dx.doi.org/10.1021/acsptsci.9b00080
ACS Pharmacol. Transl. Sci. 2020, 3, 263−284

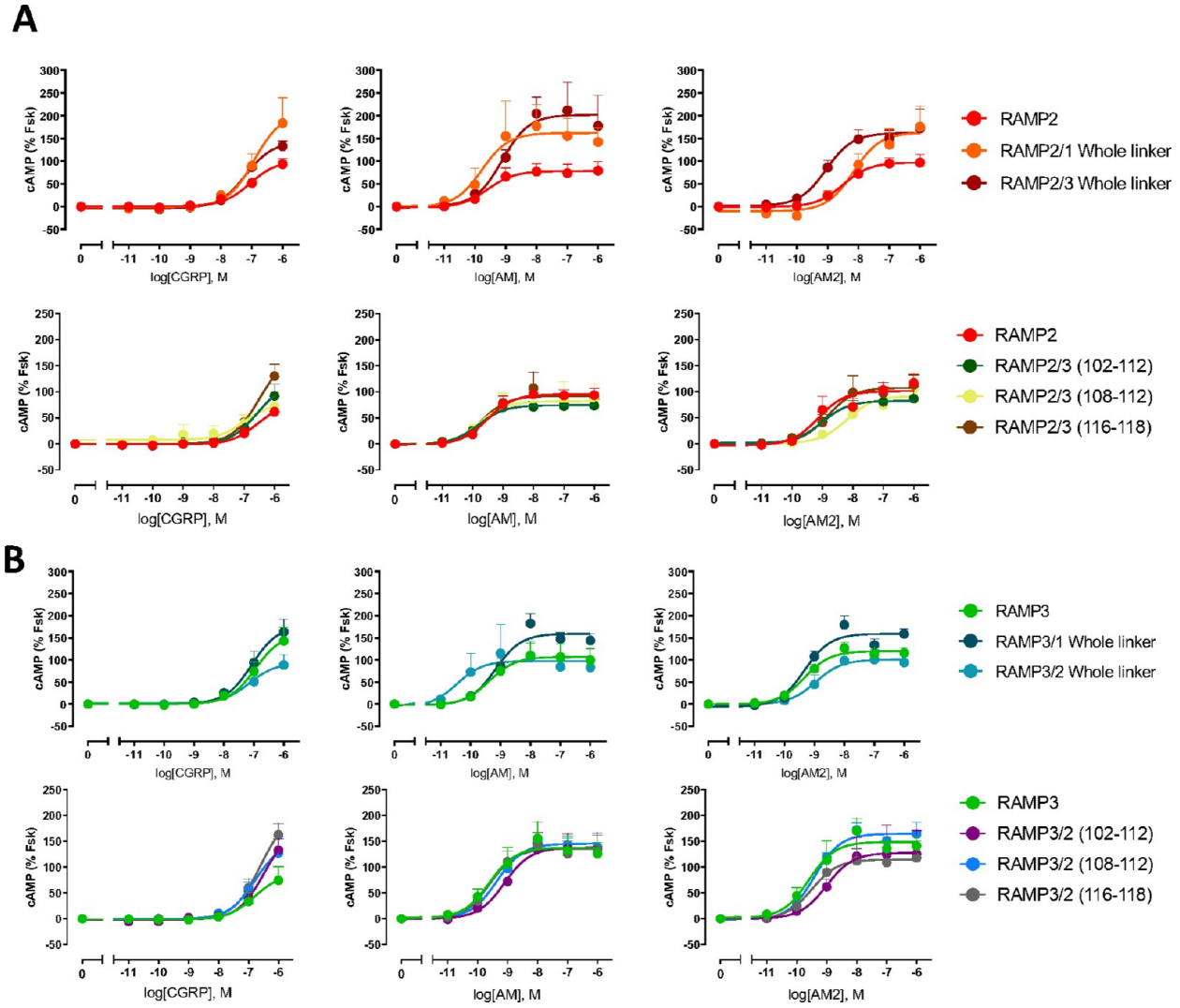

Figure 12. Pharmacological analysis of RAMP2 linker chimeras with RAMP1 or RAMP3 (A) or RAMP3 chimeras with RAMP1 or RAMP2 (B). Peptide concentration−response was measured in cAMP accumulation assay, following transient expression of constructs into COS-7 cells, for full linker exchange (A, B, upper panels) or exchange of the RAMP2 108−112 segment, the 116−118 segment, or the 102−112 segment with that of RAMP3 (A, lower panel), or exchange of the RAMP3 108−112 segment, the 116−118 segment, or the 102−112 segment with that of RAMP2 (B, lower panel).

increase in AM potency, with an apparent small decrease in AM2 potency; however, neither of these was statistically significant. Shorter exchanges of RAMP2 did not modify AM responses and had relatively minor effects on AM2 potency or E_{max} (Figure 12B; Table 1).

Overall, the pharmacological analysis of the RAMP linker chimeras provides strong evidence of involvement of this domain in the allosteric modulation of CLR phenotype, most likely due to changes to the dynamics of the RAMP−CLR interaction and subsequently the dynamics of the receptor ECDs. This is consistent with the observed distinctions in the dynamics of each of the CGRP and AM_1 and AM_2 receptors. The coordinated motions of the ECD and G protein are also indicative of a role of the ECD dynamics in G protein coupling efficiency and of an allosteric link between G protein coupling, ECD dynamics, and receptor phenotype. While this has not been studied for CLR, overexpression of different G proteins can influence binding of amylin to CTR−RAMP heterodimers.[50] As such, the current observations could provide a mechanism for how chimeric exchange of the C-terminus of RAMP1 and RAMP2 alters selective responsiveness to CGRP.[51] Moreover, biased agonism has been observed at the CLR:RAMP family of receptors, with relative potency of the peptides varying in a receptor- and pathway-dependent manner[52] suggesting that the dynamics found for Gs coupled receptors could also influence the spectrum of signaling response. Our observations are also consistent with known behavior of enzymes that exhibit dynamic allostery, whereby long-range binding information is transmitted to control catalysis.[53]

CONCLUSION

In this study, we have generated novel structures of AM receptor complexes that have provided details of the consensus modes of peptide interaction at AM_1 and AM_2 receptors. This is supported by an Ala scan of AM in our companion paper.[33] Moreover, we have used the power of cryo-EM to derive information on the dynamics of RAMP−CLR complexes demonstrating that cryo-EM can resolve aspects of the motions of highly dynamic proteins, including

https://dx.doi.org/10.1021/acsptsci.9b00080
ACS Pharmacol. Transl. Sci. 2020, 3, 263−284

GPCRs. Importantly, it was this dynamic conformational information that provided key insight into the molecular mechanism for RAMP modulation of CLR phenotypes that was subsequently experimentally verified. Thus, this work provides fundamental advances in our understanding of GPCR function and of allosteric regulation of GPCRs by large accessory proteins.

METHODS

Constructs. *Expression Constructs.* CLR was modified as previously described,[20] with replacement of the native signal peptide with that of hemagglutinin to improve expression, and inclusion of an N-terminal FLAG tag epitope and a C-terminal 8× histidine tag, each flanked by 3C protease cleavage sites (Figure S1). RAMP2 and RAMP3 were modified to replace the native signal peptide and inclusion of an N-terminal FLAG tag epitope (Figure S1). The constructs were generated in both mammalian and insect cell expression vectors as previously described.[20,23]

Constructs for Pharmacological Analyses. C-myc-tagged CLR was a gift from Dr. Steve Foord.[54] Chimeras of the RAMPs were generated by substituting different segments of the linker, between the RAMP transmembrane domain and ECD, into CD33-FLAG-tagged RAMPs in pcDNA 3.1. Short chimeras (less than 5 amino acids) were generated using single oligo mutagenesis by Q5 DNA polymerase. PCR was performed using a sense mutant oligo coding the chimeric amino acids flanked by 15 homologous nucleotides on either side. According to the protocol, 2× Q5 High Fidelity master mix (New England Biolabs) was used with 0.5 μL of 10 mM dNTPs. Reactions were treated overnight with DpnI to digest the parental WT DNA template. The long chimeras (10−16 amino acids) were generated using a nonoverlap double oligo mutagenesis method to insert the chimeric amino acids. Sense and antisense oligos were created and 5′ phosphorylated at synthesis. The sense oligos had the second half of the chimeric amino acids coded at the 5′ end, followed by the homologous sequence, and the antisense oligos had the first half of the chimeric amino acids coded at the 3′ end preceded by homologous sequence. Both oligos were added into a PCR reaction using Phusion High-Fidelity DNA polymerase and Phusion High Fidelity buffer (New England Biolabs), with the following PCR cycling protocol: 1 cycle: 2 min at 98 °C; 35 cycles: 98 °C 10 s, 55 °C 30 s, 72 °C 4 min; 1 cycle: 72 °C 5 min. The PCR reaction was treated with DpnI for 3 h to digest the parental template DNA. The blunt ends were annealed together in a 10 μL of ligation reaction (1 μL of T4 DNA ligase buffer, 1 μL of PCR reaction, 8 μL of water, 1 μL of T4 DNA ligase) for 1 h at room temperature and then at 4 °C overnight. Samples (3 μL) of all reactions were transformed in DH5α cells, and DNA was isolated from colonies through the Qiagen Miniprep kit (Venlo, Netherlands). Constructs confirmed by sequencing.

Protein Expression and Purification. CLR, RAMP2 or RAMP3, human $DNG_{\alpha s}$,[24,25] His6-tagged human Gβ1 and Gγ2 were expressed in *Tni* insect cells (Expression systems) using baculovirus. For the AM_2R complexes, the DNGs contained an additional mutation, Gαs A366S. Cell cultures were grown in ESF 921 serum-free media (Expression Systems) to a density of 4 million cells per mL and then infected with four separate baculoviruses for 48 h. Cell pellets were frozen at −80 °C until use. The cell pellet was thawed in 20 mM 4-(2-hydroxyethyl)-1-piperazineethanesulfonic acid (HEPES) pH 7.4, 50 mM NaCl, and 2 mM $MgCl_2$ supplemented with cOmplete Protease Inhibitor Cocktail tablets (Roche). Complex formation was initiated by addition of 10 μM AM or AM2 peptide (Chinapeptides), Nb35-His (10 μg/mL), 3C protease (10 μg/mL; to cleave tags from CLR), and Apyrase (25 mU/mL, NEB); the suspension was incubated for 1 h at room temperature. Membranes were collected by centrifugation at 30 000*g* for 30 min; complex from the membrane was solubilized using 0.5% (w/v) lauryl maltose neopentyl glycol (LMNG, Anatrace) supplemented with 0.03% (w/v) cholesteryl hemisuccinate (CHS, Anatrace) for 2 h at 4 °C in the presence of 1 μM of AM or AM2 peptide and Apyrase (25 mU/mL, NEB). Insoluble material was removed by centrifugation at 30 000*g* for 30 min, and the solubilized complex was immobilized by batch binding to NiNTA resin. The resin was packed into a glass column and washed with 20 column volumes of 20 mM HEPES pH 7.4, 100 mM NaCl, 2 mM $MgCl_2$, 0.01% (w/v) MNG, 0.0006% (w/v) CHS, and 1 μM AM or AM2 peptide before bound material was eluted in buffer containing 250 mM imidazole. The NiNTA purified fraction was immobilized by batch binding to M1 anti-FLAG affinity resin in the presence of 3 mM $CaCl_2$. The resin was packed into a glass column and washed with 20 column volumes of 20 mM HEPES pH 7.4, 100 mM NaCl, 2 mM $MgCl_2$, 3 mM $CaCl_2$, 1 μM AM or AM2 peptide, 0.01% (w/v) MNG, and 0.0006% (w/v) CHS before bound material was eluted in buffer containing 5 mM EGTA and 0.1 mg/mL FLAG peptide. The complex was then concentrated using an Amicon Ultra Centrifugal Filter (MWCO 100 kDa) and subjected to SEC on either a Superose 6 Increase 10/300 column (GE Healthcare) ($AM:AM_1R$, $AM2:AM_2R$), or a Superdex 200 Increase 10/300 column (GE Healthcare) ($AM:AM_2R$) that was pre-equilibrated with 20 mM HEPES pH 7.4, 100 mM NaCl, 2 mM $MgCl_2$, 1 μM AM or AM2 peptide, 0.01% (w/v) MNG, and 0.0006% (w/v) CHS. Eluted fractions consisting of receptor and G protein complex were pooled and concentrated.

SDS−PAGE and Western Blot Analysis. Samples collected from SEC were analyzed by SDS−PAGE and Western blot as previously described.[26] For SDS−PAGE, precast gradient TGX gels (Bio-Rad) were used. The final SEC elution peak was stained by Instant Blue (Expedeon).

Electron Microscopy. Samples (3 μL) were applied to acetone-prewashed, glow-discharged Quantifoil R1.2/1.3 CuRh 200 mesh holey carbon grids (Quantifoil GmbH, Großlöbichau, Germany) for AM:CLR:RAMP2:-GαsDN:Gβ1:Gγ2:Nb35 and Ultrafoil R1.2/1.3 Au 300 mesh for AM2:CLR:RAMP3:GαsDN:Gβ1:Gγ2:Nb35) and AM:CLR:RAMP3:GαsDN:Gβ1:Gγ2:Nb35. Samples were flash frozen in liquid ethane using a Vitrobot Mark IV (Thermo Fisher Scientific, Waltham, MA, USA). Data were collected on a Titan Krios microscope (Thermo Fisher Scientific, Waltham, MA, USA) operated at an accelerating voltage of 300 kV with a 50 μm C2 aperture at an indicated magnification of 105 000× in nanoprobe EFTEM mode and a spot size of 4. A Gatan K3 direct electron detector positioned post a Gatan Quantum energy filter (Gatan, Pleasanton, CA, USA), operated in a zero-energy-loss mode with a slit width of 25 eV was used to acquire dose-fractionated images of the AM_1R and AM_2R samples. Movies were recorded as compressed TIFFs in normal-resolution mode yielding a physical pixel size of 0.83 Å/pixel with an exposure time of 3.5

https://dx.doi.org/10.1021/acsptsci.9b00080
ACS Pharmacol. Transl. Sci. 2020, 3, 263−284

s amounting to a total exposure of 60−68 $e^-/Å^2$ for at an exposure rate of 13.5−20.0 e^-/pixel/second that was fractionated into 70 subframes. Defocus was varied in the range between −0.7 to −1.5 μm. Beam-image shift was used to acquire data from 9 surrounding holes after which the stage was moved to the next collection area using a custom script for the SerialEM software package.[55,56] This allowed for a higher throughput data collection, corresponding to an acquisition rate of more than 200 micrographs/hour.[57]

Data Processing. Movies were motion-corrected, dose-weighted, and integrated using UCSF MotionCor2.[58,59] This was followed by CTF estimation using the GCTF[60] software package. Particles were picked from the micrographs using the automated procedure in the crYOLO software package.[61] Particle extraction and reference-free 2D classification was carried out in RELION (version 3.0.7 for RAMP2:AM and version 3.1 for RAMP3:AM and RAMP3:AM2).[62−65] CryoSPARC (version 2.7) was used to generate an *ab initio* model of the AM:CLR:RAMP2:GαsDN:Gβ1:Gγ2:Nb35,[66] which was used in RELION for 3D classification, as well as the other two GPCR complexes. A homogeneous subset of particles was then subjected to cycles of Bayesian particle polishing and CTF refinement as implemented in RELION (See Figure S3 for cryoEM workflow on each complex). This homogeneous subset of polished particles was used for a 3D refinement in RELION and was further classified into 3D classes without angular and translational alignments, or with a fine grain angular sampling only allowing for local Euler angle searches. Particles belonging to the 3D class that yielded the best resolved map were then subjected to further 3D refinements where the α-helical domain of the Gαs protein and the detergent micelle were masked and a final 3D refinement was carried out in RELION with a mask that included the detergent micelle but not the poorly resolved α-helical domain of the G-α subunit, yielding consensus maps of the complexes with global resolutions (FSC = 0.143) of 3.0 Å (AM:CLR:RAMP2:GαsDN:Gβ1:Gγ2:Nb35), 2.3 Å (AM2:CLR:RAMP3:GαsDN:Gβ1:Gγ2:Nb35), and 2.4 Å (AM:CLR:RAMP3:GαsDN:Gβ1:Gγ2:Nb35), respectively. Local resolution estimations were performed using RELION. Additional focused refinements of the AM_2R complexes were performed through separate masking of the receptor domain using RELION[67] to yield "receptor-only" maps with global resolution of 2.6 Å for both AM_2Rs that had markedly improved local resolution of the receptor ECD.

Atomic Model Refinement. Initial models for each of the AM receptor complexes were made with the Rosetta software package using the structure threading/comparative modeling and model relaxation protocols.[68] Fitting the Rosetta generated models in the cryo-EM density maps was performed with the MDFF routine in namd2.[69] The fitted models were further refined by rounds of manual model building in coot[70] and real-space refinement, as implemented in the Phenix software package.[71] The crystal structure of the CLR:RAMP1 extracellular domain heterodimer in complex with adrenomedullin 2 (PDB: 6D1U)[28] was used as a guide for the C-terminal portion of the AM and AM2 peptides for the AM_2R models. The density around the N-terminal extracellular domains was poorly resolved for the AM_1R and was only modeled at a backbone level. Map and model statistics are detailed in Table S1.

CryoEM Dynamics Analysis. *cryoSPARC 3D Variability.* The final Polished and CTFRefined particle stacks from RELION consensus refinements were imported into the cryoSPARC environment. To ensure only highly resolved particles were analyzed, 2D classification and selection as well as a multiple volume 3D refinements were carried out. Only particles that contributed to a high-resolution refinement were further analyzed. These particles then underwent a consensus high-resolution 3D refinement, using a low-pass-filtered RELION consensus model as a starting model. A generous mask that included the detergent micelle, which had a 5 pixel map expansion and 10 pixel soft edge, was built in RELION, so any possible motions could be accounted for during the 3D variability analysis. 3D variability was then calculated as implemented in cryoSPARC (v2.9). During the variability analysis, data was considered to a resolution of 3.2 Å. The volume frame data was then generated in cryoSPARC and examined in UCSF Chimera. Output files were visualized in Chimera using the Volume Series command and captured as movies.

Interaction surfaces between peptide ligands and receptors, or those between receptors and G protein, were analyzed using the "Dimplot" module within the Ligplot+ program (v2.1).[72] Additional analyses and production of images were performed using either Molsoft ICM (v3.8−7) or the UCSF Chimera package (v1.14) from the Computer Graphics Laboratory, University of California, San Francisco (supported by NIH P41 RR-01081). Electrostatic potential calculations were performed separately on the individual proteins. Calculations were performed using the EP function, calculated by the REBEL boundary element solution of the Poisson equation, in ICMPro using default settings.[73] The scale is −5 to +5 kT e^{-1}.

Modeling. The CLR ICL3 loop was generated using PLOP[74] and minimized in the presence of Gα to eliminate steric clashes. The Gα loop between A249-N264 was modeled using the shorter loop from the adenosine A_{2A} receptor:G protein complex (PDB code 5G53).[75] Other missing loops in the G protein were added by molecular superposition from the β_2-adrenergic receptor:G protein complex (PDB code 3SN6).[27] The joining point was taken as the closest atom pairs (usually ∼0.2 Å) that maintained an appropriate Cα−Cα distance (3.7−3.9 Å) across the join; selected residues spanning the join were minimized using PLOP as necessary. The helical domain between Gα residues G47 and G207, not visible in the cryo-EM structure, was omitted.

Molecular Dynamics (MD) Simulations. The CLR:RAMP1:CGRP:Gs complex MD trajectories were produced for our previous work.[20] The CLR:RAMP2:AM:Gs complex was prepared with the CHARMM36 force field[76] using in-house scripts that combine python HTMD[77] and tcl (Tool Command Language) languages. Briefly, the PDB 2pqr[78] and propka[79] software were employed to add hydrogen atoms (considering a simulated pH of 7.0); the protonation of titratable side chains was checked by visual inspection. The resulting system was first opportunely oriented according to the CGRPR structure retrieved from the OPM database[80] and then embedded in a square 120 Å × 120 Å 1-palmitoyl-2-oleyl-*sn*-glycerol-3-phosphocholine (POPC) bilayer (previously built by using the VMD Membrane Builder plugin 1.1, Membrane Plugin, version 1.1. at http://www.ks.uiuc.edu/Research/vmd/plugins/membrane/) through an insertion method. Lipids overlapping the receptor TM bundle and the RAMP were removed and TIP3P water molecules[81] were added to the simulation box (120 Å × 120 Å × 175 Å)

https://dx.doi.org/10.1021/acsptsci.9b00080
ACS Pharmacol. Transl. Sci. 2020, 3, 263−284

utilizing the VMD Solvate plugin 1.5 (Solvate Plugin, Version 1.5. at http://www.ks.uiuc.edu/Research/vmd/plugins/solvate/). Finally, the system charge neutrality was reached by adding Na^+/Cl^- counterions (final ionic strength of 0.150 M), using the VMD Autoionize plugin 1.3 (Autoionize Plugin, Version 1.3. at http://www.ks.uiuc.edu/Research/vmd/plugins/autoionize/).

Systems Equilibration and MD Settings. ACEMD[82] was employed for both the equilibration and productive MD simulations. The equilibration steps were performed in isothermal−isobaric conditions (NPT) using the Berendsen barostat[83] (target pressure 1 atm) and the Langevin thermostat[84] (target temperature 300 K) with low damping of 1 ps^{-1}, using an integration time step of 2 fs. Clashes between protein and lipid atoms were first reduced through 2500 conjugate−gradient minimization steps, then a 2 ns long MD simulation was run with a positional restraint of 1 kcal mol^{-1} $Å^{-2}$ on protein and lipid phosphorus atoms. During a further 20 ns of MD simulation, restraints were applied only to the protein atoms, while in the last equilibration stage, positional restraints were applied only to the protein backbone alpha carbons, for a further 80 ns. Productive trajectories (12 replicas of 500 ns each, for a total simulation time of 6 μs) were computed with an integration time step of 4 fs (through hydrogen mass repartitioning)[85] in the canonical ensemble (NVT) at 300 K, using a thermostat damping of 0.1 ps^{-1} and the M-SHAKE algorithm[86] to constrain the bond lengths involving hydrogen atoms. The cutoff distance for electrostatic interactions was set at 9 Å, with a switching function applied beyond 7.5 Å. Long-range Coulomb interactions were handled using the particle mesh Ewald summation method (PME)[87] by setting the mesh spacing to 1.0 Å.

Mammalian Cell cAMP Assays. Cos7 cells, confirmed to be mycoplasma-free, were transfected in suspension in 96-well plates. The transfection was performed in 5% FBS DMEM (200 μL total volume per well) and cells were incubated for 48 h at 37 °C and 5% CO_2. For expression constructs, 10 000 cells/well were transfected with 50 ng of CLR + 50 ng of human RAMP2 or RAMP3 using 600 ng of PEI. For analysis of chimeric RAMP constructs, 15 000 cells/well were transfected with 32.5 ng of CLR + 32.5 ng of RAMP construct using 390 ng of PEI. Different chimeras were assessed as distinct batches, with a separate control wild-type RAMP included for each, due to the expression variance inherent in transient transfection. cAMP detection was performed as previously described.[88] Peptides for concentration response curves were from China Peptides. All values were converted to cAMP concentration using a cAMP standard curve performed in parallel, and data were subsequently normalized to the response of 100 μM forskolin. Data were analyzed using a 3-parameter logistic fit in Prism v8.2 (GraphPad) and assessed for differences in fitted parameters from the parental construct at 95% confidence intervals. Differences in globally fitted curves were also assessed using an extra sum of squares F-test at $P < 0.05$, with posthoc assessment of individual fitted parameters where curves were statistically different. All statistical analysis was performed in Prism v8.2.

Cell Surface Expression of Proteins: Assessment by FACS. Surface expression of c-Myc CLR or RAMP/RAMP chimeric constructs was quantified by flow cytometry analysis of antibody binding to the cMyc-tagged CLR or FLAG-tagged RAMP, respectively, using standard methods. Cos7 cells, confirmed to be mycoplasma-free, were transfected in suspension in 6-well plates. Into 450,000 cells/well was transfected 975 ng of CLR + 975 ng of RAMP construct using 11.7 mg of PEI. The transfection was performed in 5% FBS DMEM, and cells were incubated for 48 h at 37 °C and 5% CO_2. All staining steps were conducted in ice-cold Hank's Balanced Salt Solution (HBSS) with 0.1% bovine serum albumin (BSA) and 20 mM HEPES pH 7.4. Blocking was conducted in 5% BSA. Primary antibody staining was performed with 3 μg/mL 9E10 (anti-c-Myc) antibody or 1 μg/mL M2 (anti-FLAG) antibody. The secondary antibody was 1 μg/mL goat anti-mouse AF647 (ThermoFisher). Sytox blue was used for live/dead discrimination. Data were collected on a FACS CantosII (BD Biosciences). Data were analyzed using FlowJo. The mean AF647 fluorescence intensity is of live cells, and the percentage of live cells gated as positive for AF647 was against the pcDNA control.

■ ASSOCIATED CONTENT

Supporting Information

The Supporting Information is available free of charge at https://pubs.acs.org/doi/10.1021/acsptsci.9b00080.

Table S1: structure statistics; Figures S1−S10: sequences, pharmacology of the expression constructs, workflow for the consensus EM map refinements, atomic coordinates in the cryo-EM density maps, summary of atomic modelling, CLR−RAMP interface model and electrostatic surface diagrams, overview of the receptor conformation dynamic analysis, and cell surface expression of constructs (PDF)

Movies S1−S15: CryoSPARC 3D multivariate analyses S1−S3 (AM_AM_1R, full complex, normal modes 1−3), S4 (AM_AM_1R, ECL2 zoom, normal mode 1), S5 (AM_AM_1R, ICL2 zoom, normal mode 1). S6−S8 (AM_AM_2R, full complex, normal modes 1−3), S9 (AM_AM_2R, ECL2 zoom, normal mode 2), S10 (AM_AM_2R, ICL2 zoom, normal mode 3). S11−S13 (AM2_AM_2R, full complex, normal modes 1−3), S14 (AM2_AM_2R, ECL2 zoom, normal mode 1), S15 (AM2_AM_2R, ICL2 zoom, normal mode 1) (ZIP)

Movie S16: Comparative MD simulations of the CGRPR complex[20] (left panel) and the AM-bound AM_1R complex (right panel). The AM_AM_1R has greater relative motion of the ECD and the RAMP2 linker forms more transient interactions with both the receptor ECL2 and ECD than the corresponding CGRPR complex. Movie S17: Long time-scale simulation of the AM-bound AM_1R complex illustrating mobility of the full complex at 2 angles (ZIP)

Movies S18−S22: Principal component analysis of the MD simulation of the AM-bound AM_1R complex shown in Movie S17, showing the 5 main principal components in each of Movies S18−S22. The arrows track the motions in each principal component and illustrate coordinated motions between the receptor and G protein (ZIP)

■ AUTHOR INFORMATION

Corresponding Authors

Patrick M. Sexton − *Drug Discovery Biology, Monash Institute of Pharmaceutical Sciences, Monash University, Parkville 3052, Victoria, Australia; School of Pharmacy, Fudan University,*

https://dx.doi.org/10.1021/acsptsci.9b00080
ACS Pharmacol. Transl. Sci. 2020, 3, 263−284

Shanghai 201203, China; orcid.org/0000-0001-8902-2473; Email: Patrick.sexton@monash.edu

Denise Wootten − *Drug Discovery Biology, Monash Institute of Pharmaceutical Sciences, Monash University, Parkville 3052, Victoria, Australia; School of Pharmacy, Fudan University, Shanghai 201203, China*; Email: denise.wootten@monash.edu

Authors

Yi-Lynn Liang − *Drug Discovery Biology, Monash Institute of Pharmaceutical Sciences, Monash University, Parkville 3052, Victoria, Australia*

Matthew J. Belousoff − *Drug Discovery Biology, Monash Institute of Pharmaceutical Sciences, Monash University, Parkville 3052, Victoria, Australia*

Madeleine M. Fletcher − *Drug Discovery Biology, Monash Institute of Pharmaceutical Sciences, Monash University, Parkville 3052, Victoria, Australia*

Xin Zhang − *Drug Discovery Biology, Monash Institute of Pharmaceutical Sciences, Monash University, Parkville 3052, Victoria, Australia*

Maryam Khoshouei − *Department of Molecular Structural Biology, Max Planck Institute of Biochemistry, 82152 Martinsried, Germany*

Giuseppe Deganutti − *School of Biological Sciences, University of Essex, Colchester CO4 3SQ, United Kingdom;* orcid.org/0000-0001-8780-2986

Cassandra Koole − *Drug Discovery Biology, Monash Institute of Pharmaceutical Sciences, Monash University, Parkville 3052, Victoria, Australia*

Sebastian G. B. Furness − *Drug Discovery Biology, Monash Institute of Pharmaceutical Sciences, Monash University, Parkville 3052, Victoria, Australia;* orcid.org/0000-0001-8655-8221

Laurence J. Miller − *Drug Discovery Biology, Monash Institute of Pharmaceutical Sciences, Monash University, Parkville 3052, Victoria, Australia; Department of Molecular Pharmacology and Experimental Therapeutics, Mayo Clinic, Scottsdale, Arizona 85259, United States*

Debbie L. Hay − *School of Biological Sciences, and Maurice Wilkins Centre for Molecular Biodiscovery, University of Auckland, Auckland 1142, New Zealand;* orcid.org/0000-0002-9558-5122

Arthur Christopoulos − *Drug Discovery Biology, Monash Institute of Pharmaceutical Sciences, Monash University, Parkville 3052, Victoria, Australia*

Christopher A. Reynolds − *School of Biological Sciences, University of Essex, Colchester CO4 3SQ, United Kingdom*

Radostin Danev − *Graduate School of Medicine, University of Tokyo, 113-0033 Tokyo, Japan;* orcid.org/0000-0001-6406-8993

Complete contact information is available at: https://pubs.acs.org/10.1021/acsptsci.9b00080

Author Contributions

○Y.-L.L., M.J.B., and M.M.F. contributed equally to this work. Y.-L.L. developed the biochemistry for complex formation, generated purified stable complex, characterized the protein by negative stain TEM, and contributed to writing of the manuscript. M.J.B. analyzed the micrographs, generated the refined maps, generated the atomic models, completed conformational analysis on the AM receptor maps, prepared figures, and contributed to writing of the manuscript. M.M.F. completed pharmacological characterization of chimeric RAMPs, generated figures, and contributed to writing of the manuscript. X.Z. completed conformational analyses on the CGRP receptor maps and contributed to editing of the manuscript. M.K. completed initial cryo-EM imaging and analysis of the AM_1 receptor complex. G.D. and C.A.R. completed the MD simulations, contributed to analysis and interpretation of the data, and contributed to editing of the manuscript. C.K. completed pharmacological characterization of constructs and contributed to editing of the manuscript. L.J.M., S.G.B.F., D.L.H., and A.C. contributed to project development, interpretation of the data, and editing of the manuscript. R.D. developed the vitrification strategy, collected the cryo-EM data for all of the structures, contributed to analysis and interpretation of the data, and contributed to writing of the manuscript. D.W. and P.M.S. oversaw the project (including analysis and interpretation of the data), generated figures, and wrote the manuscript.

Notes

The authors declare no competing financial interest.

Cryo-EM maps are deposited in the PDB and EMDB databases with the following codes: AM:AM_1R:Gs (6UUN, EMD-20883), AM:AM_2R:Gs (6UUS, EMD-20901), and AM2:AM_2R:Gs (6UVA, EMD-20906).

■ ACKNOWLEDGMENTS

This work was supported by the Monash University Ramaciotti Centre for Cryo-Electron Microscopy, the Monash MASSIVE high-performance computing facility, the National Health and Medical Research Council of Australia (NHMRC) (project grants 1120919 and 1159006) and NHMRC program grant (1150083), the Japan Society for the Promotion of Science (JSPS, KAKENHI no. 18H06043) and Japan Science and Technology Agency (JST, PRESTO no. 18069571, and Biotechnology and Biological Sciences Research Council, UK (BBSRC, grant BB/M006883). P.M.S. and A.C. are NHMRC Senior Principal Research Fellows. D.W. is an NHMRC Senior Research Fellow. C.K. is a NHMRC CJ Martin Fellow. S.G.B.F. is an Australian Research Council Future Fellow. C.A.R. is a Royal Society Industry Fellow. The authors thank George Christopoulos and Villy Julita for technical support.

■ REFERENCES

(1) Hauser, A. S., Chavali, S., Masuho, I., Jahn, L. J., Martemyanov, K. A., Gloriam, D. E., and Babu, M. M. (2018) Pharmacogenomics of GPCR Drug Targets. *Cell 172*, 41−54.

(2) Alexander, S. P., Christopoulos, A., Davenport, A. P., Kelly, E., Marrion, N. V., Peters, J. A., Faccenda, E., Harding, S. D., Pawson, A. J., Sharman, J. L., Southan, C., and Davies, J. A. (2017) The concise guide to pharmacology 2017/18: G 697 protein-coupled receptors. *Br. J. Pharmacol. 174*, S17−S129.

(3) Hay, D. L., and Pioszak, A. A. (2016) Receptor Activity-Modifying Proteins (RAMPs): New Insights and Roles. *Annu. Rev. Pharmacol. Toxicol. 56*, 469−487.

(4) Lorenzen, E., Dodig-Crnković, T., Kotliar, I. B., Pin, E., Ceraudo, E., Vaughan, R. D., Uhlèn, M., Huber, T., Schwenk, J. M., and Sakmar, T. P. (2019) Multiplexed analysis of the secretin-like GPCR-RAMP interactome. *Sci. Adv. 5* (9), No. eaaw2778.

(5) Hay, D. L., Garelja, M. L., Poyner, D. R., and Walker, C. S. (2018) Update on the pharmacology of calcitonin/CGRP family of peptides: IUPHAR Review 25. *Br. J. Pharmacol. 175*, 3−17.

(6) Dickerson, I. M., Bussey-Gaborski, R., Holt, J. C., Jordan, P. M., and Luebke, A. E. (2016) Maturation of suprathreshold auditory

nerve activity involves cochlear CGRP-receptor complex formation. *Physiol. Rep. 4*, No. e12869.
(7) Russell, F. A., King, R., Smillie, S. J., Kodji, X., and Brain, S. D. (2014) Calcitonin gene-related peptide: physiology and pathophysiology. *Physiol. Rev. 94*, 1099−1142.
(8) Walker, C. S., Li, X., Whiting, L., Glyn-Jones, S., Zhang, S., Hickey, A. J., Sewell, M. A., Ruggiero, K., Phillips, A. R., Kraegen, E. W., Hay, D. L., Cooper, G. J., and Loomes, K. M. (2010) Mice lacking the neuropeptide alpha-calcitonin gene-related peptide are protected against diet-induced obesity. *Endocrinology 151*, 4257−4269.
(9) Russo, A. F. (2019) CGRP-Based Migraine Therapeutics: How Might They Work, Why So Safe, and What Next? *ACS Pharmacol. Transl. Sci. 2*, 2−8.
(10) Ganor, Y., Drillet-Dangeard, A. S., and Bomsel, M. (2015) Calcitonin gene-related peptide inhibits human immunodeficiency type 1 transmission by Langerhans cells via an autocrine/paracrine feedback mechanism. *Acta Physiol. 213*, 432−441.
(11) Bomsel, M., and Ganor, Y. (2017) Calcitonin Gene-Related Peptide Induces HIV-1 Proteasomal Degradation in Mucosal Langerhans Cells. *J. Virol. 91*, No. e01205.
(12) Caron, K. M., and Smithies, O. (2001) Extreme hydrops fetalis and cardiovascular abnormalities in mice lacking a functional adrenomedullin gene. *Proc. Natl. Acad. Sci. U. S. A. 98*, 615−619.
(13) Klein, K. R., and Caron, K. M. (2015) Adrenomedullin in lymphangiogenesis: from development to disease. *Cell. Mol. Life Sci. 72*, 3115−3126.
(14) Matson, B. C., Pierce, S. L., Espenschied, S. T., Holle, E., Sweatt, I. H., Davis, E. S., Tarran, R., Young, S. L., Kohout, T. A., van Duin, M., and Caron, K. M. (2017) Adrenomedullin improves fertility and promotes pinopodes and cell junctions in the peri-implantation endometrium. *Biol. Reprod. 97*, 466−477.
(15) Li, M., Schwerbrock, N. M., Lenhart, P. M., Fritz-Six, K. L., Kadmiel, M., Christine, K. S., Kraus, D. M., Espenschied, S. T., Willcockson, H. H., Mack, C. P., and Caron, K. M. (2013) Fetal-derived adrenomedullin mediates the innate immune milieu of the placenta. *J. Clin. Invest. 123*, 2408−2420.
(16) Xian, X., Sakurai, T., Kamiyoshi, A., Ichikawa-Shindo, Y., Tanaka, M., Koyama, T., Kawate, H., Yang, L., Liu, T., Imai, A., Zhai, L., Hirabayashi, K., Dai, K., Tanimura, K., Liu, T., Cui, N., Igarashi, K., Yamauchi, A., and Shindo, T. (2017) Vasoprotective Activities of the Adrenomedullin-RAMP2 System in Endothelial Cells. *Endocrinology 158*, 1359−1372.
(17) Zhang, S.-Y., Xu, M.-J., and Wang, X. (2018) Adrenomedullin 2/intermedin: a putative drug candidate for treatment of cardiometabolic disease. *Br. J. Pharmacol. 175*, 1230−1240.
(18) Cheung, B. M., and Tang, F. (2012) Adrenomedullin: exciting new horizons. *Recent Pat. Endocr., Metab. Immune Drug Discovery 6*, 4−17.
(19) Ashizuka, S., Inatsu, H., Inagaki-Ohara, K., Kita, T., and Kitamura, K. (2013) Adrenomedullin as a potential therapeutic agent for inflammatory bowel disease. *Curr. Protein Pept. Sci. 14*, 246−255.
(20) Liang, Y.-L., Khoshouei, M., Deganutti, G., Glukhova, A., Koole, C., Peat, T. S., Radjainia, M., Plitzko, J. M., Baumeister, W., Miller, L. J., et al. (2018) Cryo-EM structure of the active, Gs-protein complexed, human CGRP receptor. *Nature 561*, 492−497.
(21) Booe, J. M., Walker, C. S., Barwell, J., Kuteyi, G., Simms, J., Jamaluddin, M. A., Warner, M. L., Bill, R. M., Harris, P. W., Brimble, M. A., Poyner, D. R., Hay, D. L., and Pioszak, A. A. (2015) Structural Basis for Receptor Activity-Modifying Protein-Dependent Selective Peptide Recognition by a G Protein-Coupled Receptor. *Mol. Cell 58*, 1040−1052.
(22) Draper-Joyce, C., and Furness, S. G. B. (2019) Conformational Transitions and the Activation of Heterotrimeric G Proteins by G Protein-Coupled Receptors. *ACS Pharmacol. Transl. Sci. 2*, 285−290.
(23) Liang, Y. L., Belousoff, M. J., Zhao, P., Koole, C., Fletcher, M. M., Truong, T. T., Julita, V., Christopoulos, G., Xu, H. E., Zhang, Y., Khoshouei, M., Christopoulos, A., Danev, R., Sexton, P. M., and Wootten, D. (2020) Towards a structural understanding of class B GPCR peptide binding and activation. *Mol. Cell 77*, 656.
(24) Liang, Y.-L., Khoshouei, M., Glukhova, A., Furness, S. G. B., Zhao, P., Clydesdale, L., Koole, C., Truong, T. T., Thal, D. M., Lei, S., et al. (2018) Phase-plate cryo-EM structure of a biased agonist-bound human GLP-1 receptor-Gs complex. *Nature 555*, 121−125.
(25) Liang, Y.-L., Zhao, P., Draper-Joyce, C., Baltos, J., Glukhova, A., Truong, T. T., May, L. T., Christopoulos, A., Wootten, D., Sexton, P. M., and Furness, S. G. B. (2018) Dominant negative G proteins enhance formation and purification of agonist-GPCR-G protein complexes for structure determination. *ACS Pharmacol. Transl. Sci. 1*, 12−20.
(26) Liang, Y. L., Khoshouei, M., Radjainia, M., Zhang, Y., Glukhova, A., Tarrasch, J., Thal, D. M., Furness, S. G. B., Christopoulos, G., Coudrat, T., et al. (2017) Phase-plate cryo-EM structure of a class B GPCR-G-protein complex. *Nature 546*, 118−123.
(27) Rasmussen, S. G., DeVree, B. T., Zou, Y., Kruse, A. C., Chung, K. Y., Kobilka, T. S., Thian, F. S., Chae, P. S., et al. (2011) Crystal structure of the β2 adrenergic receptor-Gs protein complex. *Nature 477*, 549−555.
(28) Roehrkasse, A. M., Booe, J. M., Lee, S. M., Warner, M. L., and Pioszak, A. A. (2018) Structure-function analyses reveal a triple β-turn receptor-bound conformation of adrenomedullin 2/intermedin and enable peptide antagonist design. *J. Biol. Chem. 293*, 15840−15854.
(29) Wootten, D., Simms, J., Miller, L. J., Christopoulos, A., and Sexton, P. M. (2013) Polar transmembrane interactions drive formation of ligand-specific and signal pathway-biased family B G protein-coupled receptor conformations. *Proc. Natl. Acad. Sci. U. S. A. 110*, 5211−5216.
(30) Watkins, H. A., Chakravarthy, M., Abhayawardana, R. S., Gingell, J. J., Garelja, M., Pardamwar, M., McElhinney, J. M. W. R., Lathbridge, A., Constantine, A., Harris, P. W. R., Yuen, T.-Y., Brimble, M. A., Barwell, J., Poyner, D. R., Woolley, M. J., Conner, A. C., Pioszak, A. A., Reynolds, C. A., and Hay, D. L. (2016) Receptor activity-modifying proteins 2 and 3 generate adrenomedullin receptor subtypes with distinct molecular properties. *J. Biol. Chem. 291*, 11657−11675.
(31) Booe, J. M., Warner, M. L., Roehrkasse, A. M., Hay, D. L., and Pioszak, A. A. (2018) Probing the Mechanism of Receptor Activity-Modifying Protein Modulation of GPCR Ligand Selectivity through Rational Design of Potent Adrenomedullin and Calcitonin Gene-Related Peptide Antagonists. *Mol. Pharmacol. 93*, 355−367.
(32) Musa, H., Hendrikse, E. R., Brimble, M. A., Garelja, M. L., Watkins, H. A., Harris, P. W. R., and Hay, D. L. (2019) Pharmacological characterization and investigation of N terminal loop amino acids of adrenomedullin 2 that are important for receptor activation. *Biochemistry 58*, 3468−3474.
(33) Garelja, M., Au, M., Brimble, M. A., Gingell, J. J., Hendrikse, E. R., Lovell, A., Poyner, D. R., Prodan, N., Siow, A., and Sexton, P. M. et al. (2020) Molecular mechanisms of class B GPCR activation: insights from adrenomedullin receptors. *ACS Pharmacol. Transl. Sci.* DOI: 10.1021/acsptsci.9b00083.
(34) Wootten, D., Reynolds, C. A., Smith, K. J., Mobarec, J. C., Furness, S. G., Miller, L. J., Christopoulos, A., and Sexton, P. M. (2016) Key interactions by conserved polar amino acids located at the transmembrane helical boundaries in Class B GPCRs modulate activation, effector specificity and biased signalling in the glucagon-like peptide-1 receptor. *Biochem. Pharmacol. 118*, 68−87.
(35) Siu, F. Y., He, M., de Graaf, C., Han, G. W., Yang, D., Zhang, Z., Zhou, C., Xu, Q., Wacker, D., Joseph, J. S., et al. (2013) Structure of the human glucagon class B G-protein-coupled receptor. *Nature 499*, 444−449.
(36) Vohra, S., Taddese, B., Conner, A. C., Poyner, D. R., Hay, D. L., Barwell, J., Reeves, P. J., Upton, G. J., and Reynolds, C. A. (2013) Similarity between class A and class B G-protein-coupled receptors exemplified through calcitonin gene-related peptide receptor modelling and mutagenesis studies. *J. R. Soc., Interface 10*, 20120846.

(37) Woolley, M. J., Reynolds, C. A., Simms, J., Walker, C. S., Mobarec, J. C., Garelja, M. L., Conner, A. C., Poyner, D. R., and Hay, D. L. (2017) Receptor activity-modifying protein dependent and independent activation mechanisms in the coupling of calcitonin gene-related peptide and adrenomedullin receptors to Gs. *Biochem. Pharmacol. 142*, 96−110.
(38) Dal Maso, E., Zhu, Y., Pham, V., Reynolds, C. A., Deganutti, G., Hick, C. A., Yang, D., Christopoulos, A., Hay, D. L., Wang, M. W., Sexton, P. M., Furness, S. G. B., and Wootten, D. (2018) Extracellular loops 2 and 3 of the calcitonin receptor selectively modify agonist binding and efficacy. *Biochem. Pharmacol. 150*, 214−244.
(39) Dal Maso, E., Glukhova, A., Zhu, Y., Garcia-Nafria, J., Tate, C. G., Atanasio, S., Reynolds, C. A., Ramirez-Aportela, E., Carazo, J.-M., Hick, C. A., et al. (2019) The molecular control of calcitonin receptor (CTR) signaling. *ACS Pharmacol. Transl. Sci. 2*, 31−51.
(40) Wootten, D., Reynolds, C. A., Smith, K. J., Mobarec, J. C., Koole, C., Savage, E. E., Pabreja, K., Simms, J., Sridhar, R., Furness, S. G. B., et al. (2016) The GLP-1 receptor extracellular surface is a molecular trigger for biased agonism. *Cell 165*, 1632−1643.
(41) Pham, V., Zhu, Y., Dal Maso, E., Reynolds, C. A., Deganutti, G., Atanasio, S., Hick, C. A., Yang, D., Christopoulos, A., Hay, D. L., Furness, S. G. B., Wang, M. W., Wootten, D., and Sexton, P. M. (2019) Deconvoluting the Molecular Control of Binding and Signaling at the Amylin 3 Receptor: RAMP3 Alters Signal Propagation through Extracellular Loops of the Calcitonin Receptor. *ACS Pharmacol. Transl. Sci. 2*, 183−187.
(42) Watkins, H. A., Walker, C. S., Ly, K. N., Bailey, R. J., Barwell, J., Poyner, D. R., and Hay, D. L. (2014) Receptor activity-modifying protein-dependent effects of mutations in the calcitonin receptor-like receptor: implications for adrenomedullin and calcitonin gene-related peptide pharmacology. *Br. J. Pharmacol. 171*, 772−788.
(43) Lei, S., Clydesdale, L., Dai, A., Cai, X., Feng, Y., Yang, D., Liang, Y. L., Koole, C., Zhao, P., Coudrat, T., et al. (2018) Two distinct domains of the glucagon-like peptide-1 receptor control peptide-mediated biased agonism. *J. Biol. Chem. 293*, 9370−9387.
(44) Dickerson, I. M. (2013) Role of CGRP-receptor component protein (RCP) in CLR/RAMP function. *Curr. Protein Pept. Sci. 14*, 407−415.
(45) Egea, S. C., and Dickerson, I. M. (2012) Direct interactions between calcitonin-like receptor (CLR) and CGRP-receptor component protein (RCP) regulate CGRP receptor signaling. *Endocrinology 153*, 1850−1860.
(46) Barwell, J., Miller, P. S., Donnelly, D., and Poyner, D. R. (2010) Mapping interaction sites within the N-terminus of the calcitonin gene-related peptide receptor; the role of residues 23−60 of the calcitonin receptor-like receptor. *Peptides 31*, 170−176.
(47) Lau, C., Hunter, M. J., Stewart, A., Perozo, E., and Vandenberg, J. I. (2018) Never at rest: insights into the conformational dynamics of ion channels from cryo-electron microscopy. *J. Physiol. 596*, 1107−1119.
(48) Murata, K., and Wolf, M. (2018) Cryo-electron microscopy for structural analysis of dynamic biological macromolecules. *Biochim. Biophys. Acta, Gen. Subj. 1862*, 324−334.
(49) Furness, S. G. B., Liang, Y. L., Nowell, C. J., Halls, M. L., Wookey, P. J., Dal Maso, E., Inoue, A., Christopoulos, A., Wootten, D., and Sexton, P. M. (2016) Ligand-Dependent Modulation of G Protein Conformation Alters Drug Efficacy. *Cell 167*, 739−749.
(50) Morfis, M., Tilakaratne, N., Furness, S. G., Christopoulos, G., Werry, T. D., Christopoulos, A., and Sexton, P. M. (2008) Receptor activity-modifying proteins differentially modulate the G protein-coupling efficiency of amylin receptors. *Endocrinology 149*, 5423−5431.
(51) Udawela, M., Christopoulos, G., Tilakaratne, N., Christopoulos, A., Albiston, A., and Sexton, P. M. (2006) Distinct receptor activity-modifying protein domains differentially modulate interaction with calcitonin receptors. *Mol. Pharmacol. 69*, 1984−1849.
(52) Weston, C., Winfield, I., Harris, M., Hodgson, R., Shah, A., Dowell, S. J., Mobarec, J. C., Woodlock, D. A., Reynolds, C. A., Poyner, D. R., Watkins, H. A., and Ladds, G. (2016) Receptor Activity-modifying Protein-directed G protein Signaling Specificity for the Calcitonin Gene-related Peptide Family of Receptors. *J. Biol. Chem. 291*, 21925−21944.
(53) Lisi, G. P., and Loria, J. P. (2017) Allostery in enzyme catalysis. *Curr. Opin. Struct. Biol. 47*, 123−130.
(54) McLatchie, L. M., Fraser, N. J., Main, M. J., Wise, A., Brown, J., Thompson, N., Solari, R., Lee, M. G., and Foord, S. M. (1998) RAMPs regulate the transport and ligand specificity of the calcitonin-receptor-like receptor. *Nature 393*, 333−339.
(55) Mastronarde, D. N. (2018) Advanced data acquisition from electron microscopes with SerialEM. *Microsc. Microanal. 24*, 864−865.
(56) Schorb, M., Haberbosch, I., Hagen, W. J. H., Schwab, Y., and Mastronarde, D. N. (2019) Software tools for automated transmission electron microscopy. *Nat. Methods 16*, 471−477.
(57) Danev, R., Yanagisawa, H., and Kikkawa, M. (2019) Cryo-electron microscopy methodology: Current aspects and future directions. *Trends Biochem. Sci. 44*, 837−848.
(58) Li, X., Mooney, P., Zheng, S., Booth, C. R., Braunfeld, M. B., Gubbens, S., Agard, D. A., and Cheng, Y. (2013) Electron counting and beam-induced motion correction enable near-atomic-resolution single-particle cryo-EM. *Nat. Methods 10*, 584−590.
(59) Zheng, S. Q., Palovcak, E., Armache, J. P., Verba, K. A., Cheng, Y., and Agard, D. A. (2017) MotionCor2: anisotropic correction of beam-induced motion for improved cryo-electron microscopy. *Nat. Methods 14*, 331−332.
(60) Zhang, K. (2016) Gctf: Real-time CTF determination and correction. *J. Struct. Biol. 193*, 1−12.
(61) Wagner, T., Merino, F., Stabrin, M., Moriya, T., Antoni, C., Apelbaum, A., Hagel, P., Sitsel, O., Raisch, T., Prumbaum, D., et al. (2019) SPHIRE-crYOLO is a fast and accurate fully automated particle picker for cryo-EM. *Commun. Biol. 2*, 218.
(62) Scheres, S. H. W. (2015) Semi-automated selection of cryo-EM particles in RELION-1.3. *J. Struct. Biol. 189*, 114−122.
(63) Kimanius, D., Forsberg, B. O., Scheres, S. H. W., and Lindahl, E. (2016) Accelerated cryo-EM structure determination with parallelisation using GPUs in RELION-2. *eLife 5*, No. e18722.
(64) Fernandez-Leiro, R., and Scheres, S. H. W. (2017) A pipeline approach to single-particle processing in RELION. Acta Crystallogr. *D Struct. Biol. 73*, 496−502.
(65) Zivanov, J., Nakane, T., Forsberg, B. O., Kimanius, D., Hagen, W. J., Lindahl, E., and Scheres, S. H. (2018) New tools for automated high-resolution cryo-EM structure determination in RELION-3. *eLife 7*, No. e42166.
(66) Punjani, A., Rubinstein, J. L., Fleet, D. J., and Brubaker, M. A. (2017) cryoSPARC: algorithms for rapid unsupervised cryo-EM structure determination. *Nat. Methods 14*, 290−296.
(67) Nakane, T., Kimanius, D., Lindahl, E., and Scheres, S. H. W. (2018) Characterisation of molecular motions in cryo-EM single particle data by multi-body refinement in RELION. *eLife 7*, No. e36861.
(68) Leaver-Fay, A., Tyka, M., Lewis, S. M., Lange, O. F., Thompson, J., Jacak, R., Kaufman, K., Renfrew, P. D., Smith, C. A., Sheffler, W., et al. (2011) ROSETTA3: an object-oriented software suite for the simulation and design of macromolecules. *Methods Enzymol. 487*, 545−574.
(69) Chan, K. Y., Trabuco, L. G., Schreiner, E., and Schulten, K. (2012) Cryo-electron microscopy modeling by the molecular dynamics flexible fitting method. *Biopolymers 97*, 678−686.
(70) Emsley, P., Lohkamp, B., Scott, W. G., and Cowtan, K. (2010) Features and development of Coot. *Acta Crystallogr., Sect. D: Biol. Crystallogr. 66*, 486−501.
(71) Adams, P. D., Afonine, P. V., Bunkoczi, G., Chen, V. B., Davis, I. W., Echols, N., Headd, J. J., Hung, L. W., Kapral, G. J., Grosse-Kunstleve, R. W., et al. (2010) PHENIX: a comprehensive Python-

https://dx.doi.org/10.1021/acsptsci.9b00080
ACS Pharmacol. Transl. Sci. 2020, 3, 263−284

based system for macromolecular structure solution. Acta Crystallogr. *Acta Crystallogr., Sect. D: Biol. Crystallogr. 66*, 213−221.
(72) Laskowski, R. A., and Swindells, M. B. (2011) LigPlot+: multiple ligand-protein interaction diagrams for drug discovery. *J. Chem. Inf. Model. 51*, 2778−2786.
(73) Totrov, M., and Abagyan, R. (2001) Rapid boundary element solvation electrostatics calculations in folding simulations: successful folding of a 23-residue peptide. *Biopolymers 60*, 124−133.
(74) Jacobson, M. P., Pincus, D. L., Rapp, C. S., Day, T. J., Honig, B., Shaw, D. E., and Friesner, R. A. (2004) A hierarchical approach to all-atom protein loop prediction. *Proteins: Struct., Funct., Genet. 55*, 351−367.
(75) Carpenter, B., Nehmé, R., Warne, T., Leslie, A. G. W., and Tate, C. G. (2016) Structure of the adenosine A(2A) receptor bound to an engineered G protein. *Nature 536*, 104−107.
(76) Huang, J., and MacKerell, A. D. (2013) CHARMM36 all-atom additive protein force field: validation based on comparison to NMR data. *J. Comput. Chem. 34*, 2135−2145.
(77) Doerr, S., Harvey, M. J., Noé, F., and De Fabritiis, G. (2016) HTMD: High-Throughput Molecular Dynamics for Molecular Discovery. *J. Chem. Theory Comput. 12*, 1845−1852.
(78) Dolinsky, T. J., Nielsen, J. E., McCammon, J. A., and Baker, N. A. (2004) PDB2PQR: an automated pipeline for the setup of Poisson-Boltzmann electrostatics calculations. *Nucleic Acids Res. 32*, W665−W667.
(79) Olsson, M. H. M., Søndergaard, C. R., Rostkowski, M., and Jensen, J. H. (2011) PROPKA3: Consistent Treatment of Internal and Surface Residues in Empirical pK Predictions. *J. Chem. Theory Comput. 7*, 525−537.
(80) Lomize, M. A., Lomize, A. L., Pogozheva, I. D., and Mosberg, H. I. (2006) OPM: orientations of proteins in membranes database. *Bioinformatics 22*, 623−625.
(81) Jorgensen, W. L., Chandrasekhar, J., Madura, J. D., Impey, R. W., and Klein, M. L. (1983) Comparison of simple potential functions for simulating liquid water. *J. Chem. Phys. 79*, 926.
(82) Harvey, M. J., Giupponi, G., and Fabritiis, G. D. (2009) ACEMD: Accelerating Biomolecular Dynamics in the Microsecond Time Scale. *J. Chem. Theory Comput. 5*, 1632−1639.
(83) Berendsen, H. J. C., Postma, J. P. M., van Gunsteren, W. F., DiNola, A., and Haak, J. R. (1984) Molecular dynamics with coupling to an external bath. *J. Chem. Phys. 81*, 3684.
(84) Loncharich, R. J., Brooks, B. R., and Pastor, R. W. (1992) Langevin dynamics of peptides: the frictional dependence of isomerization rates of N-acetylalanyl-N'-methylamide. *Biopolymers 32*, 523−535.
(85) Hopkins, C. W., Le Grand, S., Walker, R. C., and Roitberg, A. E. (2015) Long-Time-Step Molecular Dynamics through Hydrogen Mass Repartitioning. *J. Chem. Theory Comput. 11*, 1864−1874.
(86) Forester, T. R., and Smith, W. (1998) SHAKE, rattle, and roll: Efficient constraint algorithms for linked rigid bodies. *J. Comput. Chem. 19*, 102−111.
(87) Essmann, U. P. L., Perera, L., Berkowitz, M. L., Darden, T., Lee, H., and Pedersen, L. G. (1995) A smooth particle mesh Ewald method. *J. Chem. Phys. 103*, 8577−8593.
(88) Hager, M. V., Clydesdale, L., Gellman, S. H., Sexton, P. M., and Wootten, D. (2017) Characterization of signal bias at the GLP-1 receptor induced by backbone modification of GLP-1. *Biochem. Pharmacol. 136*, 99−108.

https://dx.doi.org/10.1021/acsptsci.9b00080
ACS Pharmacol. Transl. Sci. 2020, 3, 263−284